

3. EXPLANATORY NOTES¹

Shipboard Scientific Party²

Standard procedures for both drilling operations and preliminary shipboard analyses of the material recovered during Deep Sea Drilling Project (DSDP) and Ocean Drilling Program (ODP) drilling have been regularly amended and upgraded since drilling began in 1968. In this chapter, we have assembled information that will help the reader understand the basis for our preliminary conclusions and also help the interested investigator select samples for further analysis. This information concerns only shipboard operations and analyses described in the site reports in the *Initial Reports* volume of the Leg 123 *Proceedings of the Ocean Drilling Program*. Methods used by various investigators for shore-based analyses of Leg 123 data will be detailed in the individual scientific contributions published in the *Scientific Results* volume of the *Proceedings*.

Authorship of Site Chapters

The separate sections of the site chapters were written by the following shipboard scientists (authors are listed in alphabetical order in parentheses; no seniority is necessarily implied):

Site Summary (Gradstein, Ludden)
Background and Scientific Objectives (Gradstein, Ludden)
Geologic Setting (Gradstein, Ludden)
Operations (Adamson, Gradstein, Ludden, Thompson)
Sediment Lithostratigraphy (Dumoulin, Kopaska-Merkel, Marcoux, Schott, Simmons, Thurow)
Sedimentology (Dumoulin, Kopaska-Merkel, Marcoux, Schott, Simmons, Thurow)
Biostratigraphy (Baumgartner, Bown, Gradstein, Haig, Kaminski, McMinn, Moran, Mutterlose)
Sediment Paleomagnetism (Kodama, Ogg)
Sediment-Accumulation Rates (Baumgartner, Bown, Gradstein, Haig, Kaminski, McMinn, Moran, Mutterlose)
Sediment Inorganic Geochemistry (Compton, Plank)
Organic Geochemistry (Heggie)
Sediment Physical Properties (Beaussillon, Brereton, Riggins)
Basement Lithostratigraphy (Adamson, Ishiwatari, Ludden, Plank)
Basement Petrography (Adamson, Ishiwatari, Ludden, Plank)
Basement Alteration (Adamson, Ishiwatari, Ludden, Plank)
Basement Geochemistry (Adamson, Ishiwatari, Ludden, Plank)
Basement Paleomagnetism (Kodama, Ogg)
Basement Physical Properties (Beaussillon, Brereton, Riggins)
Basement Stress Measurements (Brereton, Castillo, O'Neill)
Schlumberger Logs (Castillo, Griffiths)
Seismic Stratigraphy (Buffler)
Vertical Seismic Profiling (Bolmer, Buffler)
Heat Flow Measurements (Castillo, O'Neill)
Permeability Measurements (Castillo, O'Neill)
Summary and Conclusions (Gradstein, Ludden)

Following the text of each site chapter are summary core descriptions ("barrel sheets" and igneous-rock visual core descriptions) and photographs of each core.

Definitions

Many terms in this volume may be used in a format that is not familiar to the reader or the usage here may differ from previous DSDP-ODP formats. To make these terms more readily understandable, they are defined in this section.

Conventional Use of Time and Time-Rock Units

The subdivisions of epochs/series into early, middle, late, or lower, middle, upper have no real formal standing in stratigraphy. Lithostratigraphic (rock), chronostratigraphic (time-rock), and the geochronologic (time) units have been subdivided as follows throughout this volume:

1. Lithostratigraphic units: for rock units *lower*, *middle*, and *upper* (i.e., lowercase) are used for subdividing strata; formations, or other sections of rocks, have been subdivided on the basis of superposition only, without implying time-partitioning at the same time.

2. Chronostratigraphic units: these units imply bodies of strata formed during specific intervals of geologic time. According to convention, they are subdivided using *lower*, *middle*, and *upper*. The bases of the formal time-rock units are the stages, each of which has (or should have) a stratotype, a standard section with which other sections can be compared. Stages are conventionally grouped together into the subunits that subdivide the series. When referring to the entire subdivision of the series, *Lower*, *Middle*, and *Upper* are capitalized by convention. Otherwise, lower, middle, and upper (i.e., lowercase) are used when only a portion of the subunit (or its equivalent) is referred to, or when using the subunit in the informal sense.

3. Geochronologic units: when speaking of time, age, or of sections in the temporal sense, *early*, *middle*, and *late* are used for subdivision. The bases of the formal geochronologic units are the ages (time equivalent of stages). Like stages, ages grouped together form the time subunits that subdivide epochs. When referring to the entire subunit, *Early*, *Middle*, *Late* is capitalized, but not when only a part of the subunit, or an informal sense is implied. However, such combinations as *early Early*, *middle Early*, *late Early*, etc., are used when older, medial, or younger parts of the entire subunit are implied.

Use of Ma vs. m.y.

1. *Ma* is equivalent to and replaces m.y.B.P. (million years Before Present), e.g., 35–40 Ma.

2. *m.y.* is still used in sentences such as, "for 5 m.y. in the early Miocene," or, "5 m.y. ago the climate ...," when B.P. is not implied.

Survey Data

Survey data collected prior to Leg 123 and used for selecting sites, as well as underway geophysical data collected aboard the *JOIDES Resolution* during Leg 123, are discussed in a separate

¹ Ludden, J. N., Gradstein, F. M., et al., 1990. *Proc. ODP, Init. Repts.*, 123: College Station, TX (Ocean Drilling Program).

² Shipboard Scientific Party is as in list of participants that precedes the contents.

chapter entitled "Underway Geophysics (this volume)." The underway data include bathymetry, magnetics, seismic-reflection profiles, and sonobuoy data. Bathymetry was collected using a 3.5- and a 12-kHz Precision Depth Recorder (PDR) system and was displayed on two Raytheon recorders. Bathymetry readings were recorded every 5 min from the 12-kHz records. Depths in meters at each site were corrected for (1) the variations in sound velocity with depth using Carter (1980), and (2) the depth of the sonar dome below the rig floor (18 m). Magnetic data were collected using a Geometrics 801 proton precession magnetometer, displayed on a strip chart recorder and recorded on magnetic tape for later processing. Singlefold seismic-reflection profiles were collected using two 80-in.³ water guns as a source and a 100-m-long Teledyne streamer. These data were recorded digitally on tape using a Masscomp 561 super microcomputer and also displayed in real time in analog format on two Raytheon recorders. Some preliminary processing and display of the seismic data was done on the ship using the Masscomp system. Sonobuoy data collected at each site for velocity information were also recorded on the Masscomp system for later processing.

Drilling Characteristics

Water circulation downhole is open, hence cuttings are lost onto the seafloor and cannot be examined. The only available information about sedimentary stratification in uncored or unrecovered intervals, other than from seismic data or wireline-logging results, is from an examination of the behavior of the drill string as observed and recorded on the drilling platform. Typically, the harder a layer, the slower and more difficult it is to penetrate. However, a number of other factors determine the rate of penetration, so it is not always possible to relate drilling time directly to the hardness of the layers. For example, bit weight and revolutions per minute, recorded on the drilling recorder, influence penetration rate.

Drilling Deformation

When cores are split, many show signs of significant sediment disturbance, including the downward-concave appearance of originally horizontal bands, haphazard mixing of lumps of different lithologies (mainly at the tops of cores), and the near-fluid state of some sediments recovered from tens to hundreds of meters below the seafloor. Core deformation probably occurs during any of several steps in which the core may experience stresses sufficient to alter its physical characteristics: cutting, retrieval (with accompanying changes in pressure and temperature), and core handling on deck.

Shipboard Scientific Procedures

Numbering of Sites, Holes, Cores, and Samples

ODP drill sites are numbered consecutively from the first site drilled by the *Glomar Challenger* in 1968. A site number refers to one or more holes drilled while the ship was positioned over one acoustic beacon. Multiple holes may be drilled at a single site by pulling the drill pipe above the seafloor (out of the hole), moving the ship some distance from the previous hole, and then drilling another hole.

For all ODP drill sites, a letter suffix distinguishes each hole drilled at the same site. For example: the first hole drilled is assigned the site number modified by the suffix A, the second hole takes the site number and suffix B, and so forth. Note that this procedure differs slightly from that used by DSDP (Site 1 through 624), but prevents ambiguity between site- and hole-number designations. It is important, for sampling purposes, to distinguish among holes drilled at a site, because recovered sediments or rocks from different holes usually do not come from equivalent positions in the stratigraphic column.

The cored interval is measured in meters below seafloor (mbsf). The depth interval assigned to an individual core begins with the depth below the seafloor at which coring began and extends to the depth at which coring ended (see Fig. 1). For example, each coring interval is generally up to 9.5 m long, which is the length of a core barrel; however, coring intervals may be shorter and may not necessarily be adjacent to each other, but may be separated by drilled intervals. In soft sediments, the drill string can be "washed ahead" with the core barrel in place, but may not recover sediments, by pumping water down the pipe at high pressure to wash the sediment out of the way of the bit and up the space between the drill pipe and wall of the hole. If thin, hard, rock layers are present, then it is possible to get "spotty" sampling of these resistant layers within the washed interval, and thus have a cored interval greater than 9.5 m. In drilling hard rock, a center bit may replace the core barrel if it is necessary to drill without core recovery.

Cores taken from a hole are numbered serially from the top of the hole downward. Core numbers and their associated cored intervals in meters below seafloor usually are unique in a given hole; however, this may not be true if an interval must be cored twice because of caving of cuttings or other hole problems. Maximum full recovery for a single core is 9.5 m of rock or sediment contained in a plastic liner (6.6 cm internal diameter) plus about 0.2 m (without a plastic liner) in the core catcher (Fig. 2). The core catcher is a device at the bottom of the core barrel that prevents the core from sliding out when the barrel is being retrieved from the hole. In certain situations (e.g., when coring gassy sediments that expand while being brought on deck) recovery may exceed the 9.5-m maximum.

A recovered core is divided into 1.5-m sections that are numbered serially from the top (Fig. 2). When full recovery is obtained, the sections are numbered from 1 through 7, while the last section may be shorter than 1.5 m (rarely, an unusually long core may require more than seven sections). When less than full recovery is obtained, there will be as many sections as needed to accommodate the length of the core recovered; for example, 4 m of core would be divided into two 1.5-m sections and a 1-m section. If cores are fragmented (recovery less than 100%), sections are numbered serially and intervening sections are noted as void, whether shipboard scientists believe that the fragments were contiguous *in situ* or not. In rare cases a section of less than 1.5 m may be cut to preserve features of interest (e.g., lithological contacts).

By convention, material recovered from the core catcher is placed below the last section when the core is described and is labeled core catcher (CC); in sedimentary cores, it is treated as a separate section. The core catcher is placed at the top of the cored interval in cases where material is only recovered in the core catcher. However, information supplied by the drillers or by other sources may allow for more precise interpretation as to the correct position of core-catcher material within an incompletely recovered cored interval.

A recovered basalt, gabbro, or peridotite core also is cut into 1.5-m sections that are numbered serially; however, each piece of rock is then assigned a number (fragments of a single piece are assigned a single number, with individual fragments being identified alphabetically). The core-catcher sample is placed at the bottom of the last section and is treated as part of the last section, rather than separately. Scientists completing visual core descriptions describe each lithologic unit, noting core and section boundaries only as physical reference points.

When, as is usually the case, the recovered core is shorter than the cored interval, the top of the core is equated with the top of the cored interval by convention to achieve consistency in handling analytical data derived from the cores. Samples removed from the cores are designated by distance measured in

core are sought as sites for gas sampling. Some of the gas samples are stored for shorebased study, but others are analyzed immediately as part of the shipboard safety and pollution-prevention program. Next, the core is marked into section lengths, each section is labeled, and the core is cut into sections. Interstitial-water (IW), organic geochemistry (OG), and physical properties (PP) whole-round samples are then taken. In addition, some headspace gas samples are scraped from the ends of cut sections on the catwalk, and sealed in glass vials for light hydrocarbon analysis. In places, 20-cm³ samples are taken using a syringe for pore fluid analyses. Each section is then sealed at the top and bottom by gluing on color-coded plastic caps, blue to identify the top of a section and clear for the bottom. A yellow cap is placed on section ends from which a whole-round sample has been removed. The caps are usually attached to the liner by coating the end liner and the inside rim of the cap with acetone, and then the caps are taped to the liners.

The cores then are carried into the laboratory, where the sections are again labeled, using an engraver to mark the full designation of the section. The length of the core in each section and the core-catcher sample are measured to the nearest centimeter; this information is logged into the shipboard CORELOG database program.

Next, the whole-round sections are run through the GRAPE (gamma-ray attenuation porosity evaluator) and *P*-wave logger devices to estimate the bulk density, porosity, and sonic velocity. Magnetic susceptibility measurements follow. After the core has equilibrated to room temperature (this took approximately 15 hr during Leg 123), thermal-conductivity measurements are performed immediately before the cores are split.

Cores of relatively soft material are split lengthwise into working and archive halves. The softer cores are split with a wire or saw, depending on the degree of induration. Harder cores are split with a band saw or diamond saw. As Leg 123 cores were split with wire from the bottom to top, older material may have been transported up the core on the split face of each section. Thus, one should be aware that the near-surface part of a split core might be contaminated.

The working half is sampled for both shipboard and shore-based laboratory studies. Each extracted sample is logged in the sampling computer database program by its location and the name of the investigator receiving the sample. Records of all removed samples are kept by the curator at ODP (Gulf Coast Repository). The extracted samples are sealed in plastic vials or bags and labeled. Samples are routinely taken for shipboard physical property analyses, for percentages of calcium carbonate present (coulometric analysis), and for other purposes. Many of these data are reported in the site chapters.

The archive half is described visually. Smear slides are made from samples taken from the archive half and are supplemented by thin sections taken from the working half. Archive-half sections that show little drilling disturbance are run through the cryogenic magnetometer. The archive half is then photographed with both black-and-white and color film, a whole core at a time. Close-up black-and-white photographs are taken of particular features for illustrations in the summary of each site.

Both halves of the core are then placed into labeled plastic tubes, sealed, and then transferred to cold-storage space aboard the drilling vessel. At the end of the leg, the cores are transferred from the ship in refrigerated airfreight containers to cold storage at the Gulf Coast Repository at the Ocean Drilling Program, Texas A&M University, College Station, Texas.

Igneous Rocks

Igneous rock cores are handled differently from the sedimentary cores. Once on deck, the core catcher is placed at the bottom of the core liner and total core recovery is calculated by

shunting the rock pieces together and measuring to the nearest centimeter; this information is logged into the shipboard core-log database program. The core is then cut into 1.5-m-long sections and transferred to the laboratory. Magnetic susceptibility measurements are performed using the whole-round cores before being split.

The contents of each section are transferred into 1.5-m-long sections of the split core liner, where the bottom of oriented pieces (i.e., pieces that clearly could not have rotated top to bottom about a horizontal axis in the liner) are marked with a red wax pencil. This is to ensure that orientation is not lost during splitting and labeling. An attempt is made to reconstruct the core by placing integral pieces together; a petrologist then decides on the orientation of each cut so as to preserve unique features and/or to expose important structures. Each oriented piece is then wrapped in plastic and a tracing made of the veins on the exterior surface for later correlation with the borehole televiewer. The core is then split into archive and working halves. A plastic spacer is used to separate individual pieces, and/or reconstructed groups of pieces, in the core liner. These spacers may represent a substantial interval of no recovery. Each piece is numbered sequentially from the top of each section, beginning with number 1; reconstructed groups of pieces are assigned the same number, but are lettered consecutively. Pieces are labeled on the rounded, not sawn surfaces. If the piece is oriented, an arrow is added to the label pointing to the top of the section.

The working half of the core is sampled for shipboard laboratory studies. Records of all samples are kept by the curator at ODP. Minicore samples are routinely collected for physical properties and magnetic studies; these are later subdivided for X-ray fluorescence (XRF) analysis and thin sectioning, ensuring that as many measurements as possible are performed on the same pieces of rock. At least one minicore is collected per lithologic unit when recovery permits, generally from the freshest areas of core. Additional thin sections, X-ray diffraction (XRD) samples, and XRF samples are selected from areas of particular interest. Samples for shore-based studies are selected in a sampling party held after drilling has terminated.

The archive half of the core is described visually, then photographed with both black-and-white and color film, one core at a time. Both halves of the core are then shrink-wrapped in plastic to prevent rock pieces from vibrating out of sequence during transit, put into labeled plastic tubes, sealed, and transferred to cold-storage space aboard the drilling vessel.

CORE DESCRIPTION FORMS

Sediment "Barrel Sheets"

The core description forms (Fig. 3), or "barrel sheets," summarize the data obtained during shipboard analysis of each sediment core, which have been recorded in detail on a section-by-section basis on these forms (or UCDs). Information recorded on the UCDs is available as a searchable database through the ODP Data Librarian (see notes on hard-rock core description, below). The following discussion explains the ODP conventions used for compiling each part of the core description forms and the exceptions to these procedures adopted by Leg 123 scientists.

Core Designation

Cores are designated using leg, site, hole, and core number and type as previously discussed (see "Numbering of Sites, Holes, Cores, and Samples" section, this chapter). In addition, the cored interval is specified in terms of meters below seafloor (mbsf). Depths in meters below sea level (mbsl) can be calculated by adding water depth to mbsf. Water depth for Site 765 was calculated as 5713.8 m and for Site 766 as 3997.5 m by sub-

SITE		HOLE				CORE		CORED INTERVAL					
TIME-ROCK UNIT	BIOSTRAT. ZONE/ FOSSIL CHARACTER				PALEOMAGNETICS	PHYS. PROPERTIES	CHEMISTRY	SECTION	METERS	GRAPHIC LITHOLOGY	DRILLING DISTURB. SED. STRUCTURES	SAMPLES	LITHOLOGIC DESCRIPTION
	FORAMINIFERS	NANNOFOSSILS	RADIOLARIANS	DIATOMS									
								0.5 1 1.0					
								2				PP ← Physical-properties whole-round sample	
								3				OG ← Organic geochemistry sample	
								4					Smear slide summary (%): Section, depth (cm) M = Minor lithology, D = Dominant lithology
								5				IW ← Interstitial-water sample	
								6				* ← Smear slide	
								7				G ← Headspace gas sample	
								CC					

PRESERVATION:
 G = Good
 M = Moderate
 P = Poor

ABUNDANCE:
 A = Abundant
 C = Common
 F = Frequent
 R = Rare
 B = Barren

Velocity (v), porosity (φ), and density (γ)
 Carbonate (%)

See key to graphic lithology symbols (Fig. 4)
 See key to symbols (Fig. 5)

Figure 3. Core description form ("barrel sheet") used for sediments and sedimentary rocks.

tracting estimated distance between rig floor and sea level from bottom-felt depth below rig floor. Error in the estimate of water depth from pipe bend at ship level and differential ship loading during coring as well as other sources of error may amount to ± 10 m or more.

Paleontological Data

Microfossil abundance, preservation, and zone assignment, as determined by the shipboard paleontologists, appear on the core description form under the heading "Biostrat. Zone/Fossil Character." The chronostratigraphic unit, as recognized on the basis of paleontological results, is shown in the "Time-Rock Unit" column. Detailed information on the zonations and terms used to report abundance and preservation is presented in the "Biostratigraphy" section (this chapter).

Paleomagnetic, Physical Property, and Chemical Data

Columns are provided on the core description form to record paleomagnetic results (normal, reversed, or indeterminate polarity, shown as "N," "R," or "INT," respectively), physical-property values (density, porosity, and velocity) and chemical data (percentages of CaCO_3 and total organic carbon determined using the Coulometrics analyzer). Additional information on shipboard procedures for collecting these types of data appears in the "Paleomagnetism," "Physical Properties," and "Inorganic Geochemistry" sections (this chapter).

Graphic Lithology Column

The lithological classification scheme of Mazzullo, Meyer, and Kidd (1988), accepted for shipboard use by the JOIDES Sediments and Ocean History Panel, is presented here with minor modifications. Sediment type is represented graphically on the core description forms using the symbols illustrated in Figure 4.

Sediment Disturbance

In some cases, the coring technique, which uses a 25-cm-diameter bit having a 6-cm-diameter core opening, may result in varying degrees of disturbance of the recovered core material. This is illustrated in the "Drilling Disturbance" column on the core description form (using the symbols in Fig. 5). The following disturbance categories are recognized for soft and firm sediments:

1. Slightly deformed: bedding contacts are slightly bent.
2. Moderately deformed: bedding contacts have undergone extreme bowing.
3. Highly deformed: bedding is completely disturbed, sometimes showing symmetrical diapirlike structures ("flow-in").
4. Soupy: intervals are water-saturated and have lost all aspects of original bedding.

The following categories are used to describe the degree of fracturing in hard sediments and igneous and metamorphic rocks (Fig. 5):

1. Slightly fractured: core pieces are in place and have very little drilling slurry or breccia.
2. Moderately fragmented: core pieces are in place or partly displaced, but original orientation is preserved or recognizable. Drilling slurry may surround fragments.
3. Highly fragmented: pieces are from the interval cored and probably in correct stratigraphic sequence (although they may not represent the entire section), but original orientation is totally lost.
4. Drilling breccia: core pieces have completely lost their original orientation and stratigraphic position and may be completely mixed with drilling slurry.

Sedimentary Structures

In the soft and even in some harder sedimentary cores, distinguishing between natural structures and those created by coring may be extremely difficult. However, where such structures were observed, they are indicated on the "Sedimentary Structure" column of the core description forms. A key to the structural symbols used for Leg 123 is given in Figure 5.

Color

Colors of sediment are determined by comparison with the Munsell Soil Color Chart (1975). Colors were determined immediately after the cores were split and while they were still wet. Hard rocks, such as limestones, were wetted before their color was determined.

Samples

The positions of samples taken from each core for shipboard analysis are indicated in the "Samples" column on the core description form. An asterisk (*) indicates the location of smear slide samples, a number sign (#) indicates the location of thin sections. The symbols IW, OG, and PP, designate whole-round interstitial-water, frozen organic geochemistry, and physical-properties samples, respectively. The symbols XRD and XRF indicate X-ray diffraction and X-ray fluorescence samples, respectively.

Although not indicated in the "Samples" column, the position of samples for routine physical-property (porosity [%], wet-bulk density [g/cm^3], and velocity [m/s]) and geochemical (% organic carbon [OC]) analyses are indicated by a dot and values of determination in both the "Physical Properties" column and in the "Chemistry" column. Paleomagnetic results (normal and reversed polarity intervals) are also indicated.

Shipboard paleontologists generally base their age determinations on core-catcher samples, although additional samples from other parts of the core may be examined when required. Examination of such samples may lead to the recognition of zonal boundaries in the core; these are indicated in the appropriate column. All paleontological samples are indicated, even if they are barren.

Lithologic Description—Text

The lithologic description that appears on each core description form generally consists of two parts: (1) a brief summary of the major lithologies observed in a given core, followed by a description of sedimentary structures and features, and (2) a description of minor lithologies observed in the core, including data regarding color, occurrence in the core, and significant features. A summary of features characterizing the core as a whole is sometimes included.

Smear Slide Summary

A table summarizing smear slide data appears on each core description form. The section and interval from which the sample was taken are noted, as well as identification as a dominant (D) or minor (M) lithology in the core. The percentage of all identified components is indicated. As explained in the following "Sediment Classification" section (this chapter), these data are used to classify the recovered material.

Igneous Rock "Visual Core Descriptions"

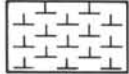
Representation of igneous rocks on barrel sheets is too compressed to provide adequate information for potential sampling. Consequently, visual core description forms, modified from those used aboard ship, are used for more complete graphic representation (Fig. 6). A description form is produced for each section of core. Copies of these forms are available on microfilm at all three ODP repositories.

GRANULAR SEDIMENTS

PELAGIC SEDIMENTS

Calcareous

Nannofossil Ooze



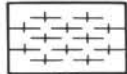
CB1

Foraminiferal Ooze



CB2

Nanno-Foram or Foram-Nanno Ooze



CB3

Calcareous Ooze



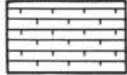
CB4

Nannofossil Chalk



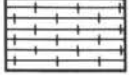
CB5

Foraminiferal Chalk



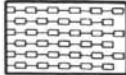
CB6

Nanno-Foram or Foram-Nanno Chalk



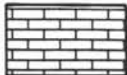
CB7

Calcareous Chalk



CB8

Limestone



CB9

Carbonate Conglomerate



AS11

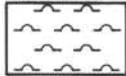
Siliceous

Diatom Ooze



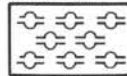
SB1

Radiolarian Ooze



SB2

Diatom-Rad or Siliceous Ooze



SB3

Diatomite



SB4

Radiolarite



SB5

Porcellanite



SB6

Chert



SB7

Spiculite



SB8

SILICICLASTIC SEDIMENTS

Clay/Claystone



T1

Shale (fissile)



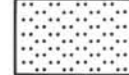
T3

Sand/Silt/Clay



T4

Silt/Siltstone



T5

Sand/Sandstone



T6

Silty/Sand/Sandy Silt



T7

Silty Clay/Clayey Silt



T8

Sandy Clay/Clayey Sand



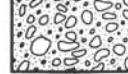
T9

Gravel



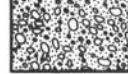
SR1

Conglomerate



SR2

Breccia



SR3

VOLCANICLASTIC SEDIMENTS

Volcanic Ash/Tuff



V1

Volcanic Lapilli



V2

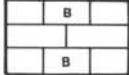
Volcanic Breccia



V3

NERITIC SEDIMENTS

Boundstone



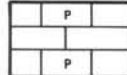
N1

Grainstone



N2

Packstone



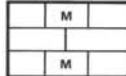
N3

Wackestone



N4

Mudstone



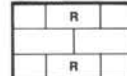
N5

Floatstone



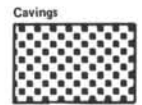
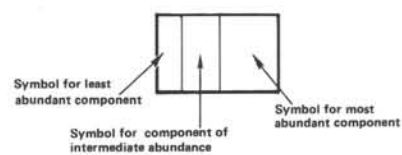
N6

Rudstone



N7

MIXED SEDIMENTS



AS9

Coals and Peat



SR6

Sapropels



SR9

Halite



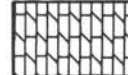
E1

Anhydrite



E2

Gypsum



E3

Porcellanite



SB6

Chert



SB7

Dolomite



SR7

Rhodochrosite



AS2

Zeolite



AS8

Concretions

Mn= Manganese

B= Barite

P= Pyrite

Z= Zeolite

drawn circle with symbol (others may be designated)

CHEMICAL SEDIMENTS

SPECIAL ROCK TYPES

Basic Igneous



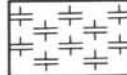
SR4

Acid Igneous



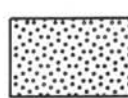
SR5

Metamorphics



SR6

ADDITIONAL SYMBOLS



AS1



AS3



AS4



AS5



AS6



AS7



AS10



AS12

Figure 4. Key to symbols used in the "graphic lithology" column on the core description form shown in Figure 3.

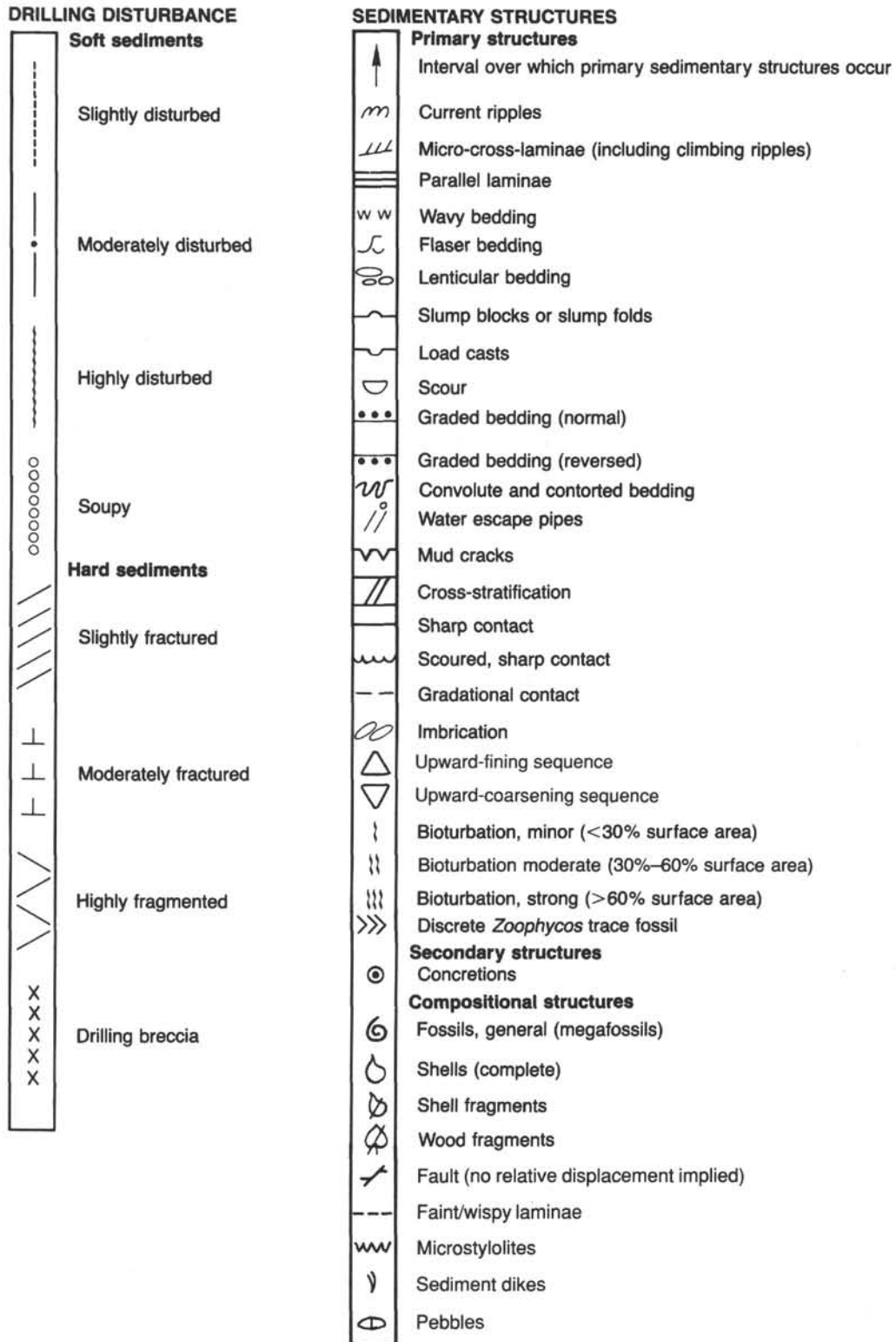
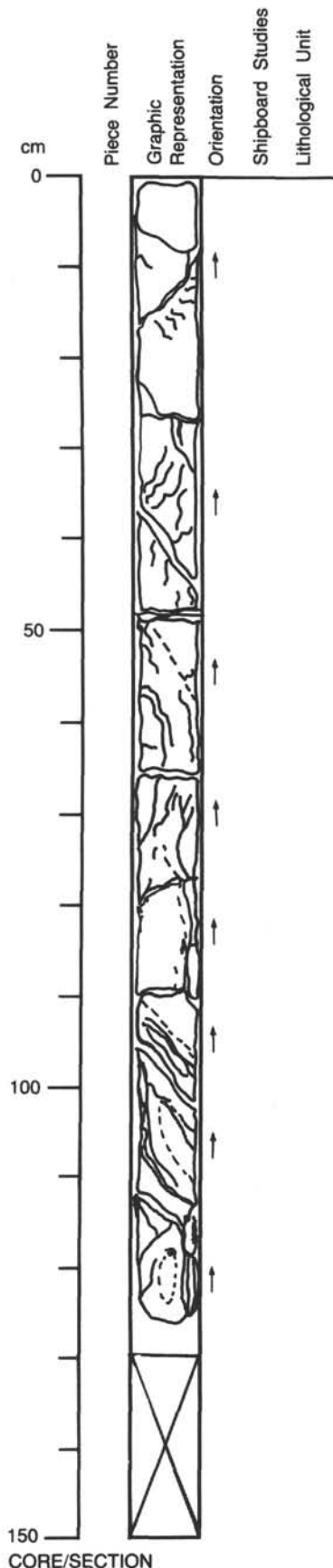


Figure 5. Symbols used for drilling disturbance and sedimentary structures on core description forms (barrel sheets). A vertical line may be added to the top of an upward-fining sequence symbol to indicate that grading is not observed in the interval indicated by the vertical line, but that this interval is inferred to belong to the same depositional event as the lower, visibly graded, portion.

123-765D-24R-2

UNIT 17: MASSIVE APHYRIC BASALT FLOWS

Pieces 24R-1,1A through 24R-3,1C (Flow B)



CONTACTS: Top contact not seen. Lower contact in Piece 24R-3, 1C: Chilled to very fine-grained, altered, buff colored to gray patchy basalt.

PHENOCRYSTS: Aphyric; well crystallized. Rare, mm sized clinopyroxene phenocrysts.

GROUNDMASS: Equigranular 1 mm. Between fine and medium-grained.

VESICLES: <1%, <1 mm, filled with black-dark green minerals. Pieces 24R-2, 2E and 2F filled with calcite.

COLOR: Gray-brown

STRUCTURE: Basalt flows.

ALTERATION: Alteration halos around veins, Piece 24R-1, 10: Brown stains not spatially related to veins. Piece 24R-1, 1E is notably fresh in lower two thirds.

VEINS/FRACTURES: Pieces 24R-1, 1A and 1E: <1-3 mm wide, essentially devoid of fractures or veins. Pieces 24R-1, 1C-1D: Calcite veins and feathery vein. Piece 24R-1, 1B: <1 mm multi-color veins.

ADDITIONAL COMMENTS: Pieces 24R-2, 1A-2F: Pronounced increase in staining/alteration toward base of section and into Section 24R-3; Pieces 24R-2, 1A-1E do not have alteration halos around veins, whereas Pieces 24R-2, 2A-2F have extensive centimeter thick halos about all veins. Lower contact is chilled to very fine-grained, and altered to a buff color. Grey patches outside the alteration halos appear to be bleached. Halos are extensive and up to centimeters in width; brown stains permeate 80% of Pieces 24R-3, 1A and 1B. Piece 24R-3 is brown to buff and chilled. It is similar to Piece 1C, but set in calcite matrix.

Figure 6. Visual core description form used for igneous rocks.

Core Designation

Cores are designated using leg, site, hole, and core number and type, as previously discussed. Unlike the sedimentary barrel sheets, the cored interval is not usually entered on the igneous visual core descriptions.

Piece Number, Graphic Representation, and Orientation

Each piece of rock is depicted as accurately as possible in the "Graphic Representation" column, together with any salient features considered worth recording, e.g., the position of veins, fractures, xenocrysts, etc. The location of glass margins are marked by heavy shading and the presence of chilled spherulitic textures by parallel hatched lines. Piece numbers are entered in the "Piece Number" column and orientation arrows, where appropriate, in the "Orientation" column.

Shipboard Studies

The position of shipboard samples is indicated in the column headed "Shipboard Studies," using the following notation:

XRD	= X-ray diffraction analysis
XRF	= X-ray fluorescence analysis
PM	= magnetic measurements
TS	= thin section
PP	= physical property measurements
TC	= thermal conductivity measurements

Thermal conductivity measurements were performed on pieces of half core and required that the sawn surface be covered with a conducting grease.

Lithological Unit

The core is divided into individual cooling units (e.g., individual pillows, individual massive flows, hyaloclastite breccias, etc.) wherever possible by using the criteria of changing grain size, occurrence of glassy margins, changes in petrographic type, and phenocryst abundances. The core is then further divided into lithological units representing eruptive cycles or specific events that may comprise one or more individual cooling units, e.g., several tens of meters of pillow basalts or several consecutive massive flows. Some lithological units are based on shipboard geochemical analysis of basement samples. The lithological units are numbered consecutively downhole, starting with Unit 1 at the top and are entered as bold numbers in the "Lithological Unit" column; contacts between lithological units are marked by a horizontal line joining the "Graphic Representation" and "Lithological Unit" columns. The contacts between individual flows or individual pillows constituting a lithological unit are marked by shorter horizontal lines in the "Lithological Unit" column; these cooling units are numbered sequentially within each lithological unit and are entered as circled numbers in the "Lithological Unit" column. Where appropriate, an arrow shows the direction of increasing grain size within each cooling unit.

Descriptions of each cooling unit within a section, or of each section, whichever is shorter, are presented to the right of the "Lithological Unit" column. The descriptive system used is discussed below.

Lithologic Description

Lithologic descriptions were prepared in a systematic way, ensuring that all important features (e.g., nature of contacts, distribution and percentage of phenocrysts, groundmass texture, color, vesicle content, alteration, etc.) were noted for each unit described.

Macroscopic Core Descriptions

Igneous rocks are classified mainly on the basis of mineralogy and texture. When describing the cores, a checklist of macroscopic features is followed to ensure consistent and complete descriptions. Two checklists, one for extrusive rocks and dikes, and one for plutonic rocks, are used by ODP, but as only extrusive rocks were recovered during Leg 123, only this checklist is presented below. The checklist for plutonic rocks is presented in the Leg 106/109 "Introduction and Explanatory Notes" (Shipboard Scientific Party, 1988).

The data on these forms go directly into a computerized database that is accessible to the entire scientific community 1 yr after the cruise.

Fine-Grained and Medium-Grained Extrusives and Dikes

The following are steps for describing extensive rocks and dikes: enter leg, site, hole, core number and type, and section information. Draw the graphic representation of the core; number the rock pieces; show orientation arrows; and record positions of shipboard samples (see Fig. 6).

Subdivide the core into cooling units, using the criteria of changing grain size, occurrence of glassy margins, and changes in petrographic type and phenocryst abundances.

For each unit, note the following:

1. Enter UNIT number (consecutive downhole), including piece numbers of top and bottom pieces in unit.
2. ROCK NAME (to be filled in last).
3. CONTACT TYPE (e.g., intrusive; discordant; depositional, etc.). Note the presence of glass and its alteration products (in %), give the azimuth and dip of the contact.
4. PHENOCRYSTS: determine if homogeneous or heterogeneous distribution; if heterogeneous distribution, note variations.
 - i. abundance (%)
 - ii. average size in mm
 - iii. shape
 - iv. percent degree of alteration and replacing phases and their relationships
 - v. further comments
 - vi. fill in 2. ROCK NAME
5. GROUNDMASS: glassy, microcrystalline, fine-grained (<1 mm), medium-grained (1–5 mm), or coarse-grained (>5 mm). Note the relative grain size changes within the unit (e.g., coarsening from Piece 1 to Piece 5).
6. COLOR (dry).
7. VESICLES: give percent, size, shape, fillings and their relationship (include % of vesicles that are filled by alteration minerals), and distribution.
8. STRUCTURE: massive, pillow lava, thin flow, breccia, etc., and comments.
9. ALTERATION: fresh (<2% altn), slightly (2%–10% altn), moderately (10%–40% altn), highly (40%–80% altn), very highly (80%–95% altn) or completely (95%–100% altn) altered. Type, form, and distribution of alteration.
10. VEINS/FRACTURES: percent present, width, orientation, fillings and relationships, halos.

Basalt Classification

Basalts are termed aphyric, sparsely phyric, moderately phyric, or highly phyric, depending upon the proportion of phenocrysts visible with the hand lens or binocular microscope (approximately 10X). Basalts are described as aphyric if phenocrysts clearly amount to less than 1% of the rock, sparsely phyric if phenocryst content ranges from 1%–2%, moderately phyric at

2%–10%, and highly phryic if phenocrysts amount to more than 10% of the rock. Basalts are further classified by phenocryst type (e.g., a moderately plagioclase-olivine phryic basalt contains 2%–10% phenocrysts, most of them plagioclase, but with some olivine).

Once the lithologic description is agreed upon by the shipboard petrologists, and the lithological units are defined, the final core description is assembled on a visual core description form (Fig. 6). These visual core description forms are published in the *Initial Reports* volume of the *Proceedings of the Ocean Drilling Program*.

Thin Section Descriptions

Thin section billets of basement rocks recovered during Leg 123 were examined to help define unit boundaries indicated by hand-specimen core descriptions, to confirm the identity of the petrologic groups represented in the cores, and to define their secondary mineralogy. At least one thin section was made of each unit identified in hand specimen, where sufficient rock was available.

The rationale for the assignment of unit boundaries, based on modal mineralogy and bulk-rock geochemistry, is presented in the basement lithostratigraphic summary (this volume). Percentages of individual mineral phases were estimated visually and are reported on the detailed thin section description sheets published in this volume. Modal abundances determined by area counting are reported in the petrography section of each site chapter. ("Area" counting, as opposed to "point" counting, uses a glass slide on which is marked a 1-mm grid, 1- × 1-cm square. This slide is placed over a thin section and the numbers of 1-mm squares occupied by each mineral are counted. The modal abundance is then calculated. This method is more rapid than point counting.) For the thin-section modal estimates, the terms sparsely, moderately, and highly abundant are used in the same manner as for hand specimen descriptions. In cases where discrepancies arise over the composition and abundance of mineral phases between hand specimen and thin section analyses, thin section descriptions are used in the lithostratigraphic summary.

Basement Alteration

Alteration effects from seawater interaction with igneous rocks were described in hand specimens and thin sections. The width and color of alteration halos around fractures or vugs were noted in the core descriptions. The identities of secondary minerals filling fractures, vesicles, and replacing igneous phases are estimated in core descriptions and refined in thin section, augmented in some cases by XRD and later electron microprobe analyses performed on shipboard thin sections. The total percentages of the various secondary minerals are also estimated from thin section examinations.

SEDIMENT CLASSIFICATION

The new classification scheme for the Ocean Drilling Program (Mazzullo, Meyer, and Kidd, 1988), partly reproduced below, was used with minor modification during Leg 123. This classification scheme defines two basic sediment types: (1) granular and (2) chemical. A significant portion of the sediments recovered during Leg 123 are composed largely of redeposited pelagic grains. The classification scheme proposed by Mazzullo, Meyer, and Kidd does not properly convey the textural information that is important for this class of sediment. Therefore, it was necessary to modify the classification scheme to reflect the character of these sediments.

Granular Sediments

Classes of Granular Sediments

Four types of grains comprise granular sediments: pelagic, neritic, siliciclastic, and volcanoclastic grains. Pelagic grains are composed of the skeletal debris of open-marine siliceous and calcareous microfauna and microflora (e.g., radiolarians or nanofossils) and associated organisms. Neritic grains are composed of calcareous skeletal debris (e.g., bioclasts) and calcareous grains of nonpelagic origin. These sediments were encountered in very small amounts during Leg 123 and are discussed only briefly. Siliciclastic grains are composed of mineral and rock fragments that were derived from plutonic, sedimentary, and metamorphic rocks. Volcanoclastic grains are composed of rock fragments and minerals that were derived from volcanic sources.

Variations in the relative proportions of these four grain types define five major classes of granular sediments: pelagic, neritic, siliciclastic, volcanoclastic, and mixed sediments (Fig. 7).

Pelagic sediments are composed of more than 60% pelagic and neritic grains and less than 40% siliciclastic and volcanoclastic grains. Pelagic grains are volumetrically more important than neritic grains.

Neritic sediments are composed of more than 60% pelagic and neritic grains and contain a higher proportion of neritic than pelagic grains.

Siliciclastic sediments are composed of more than 60% siliciclastic and volcanoclastic grains, and siliciclastic grains dominate volumetrically.

Volcanoclastic sediments are likewise composed of more than 60% siliciclastic and volcanoclastic grains, but volcanoclastic grains dominate. This class includes epiclastic sediments (volcanic detritus that is produced by erosion of volcanic rocks by wind, water, and ice), pyroclastic sediments (products of the degassing of magmas), and hydroclastic sediments (products of the granulation of volcanic glass by steam explosions). Lastly, mixed sediments contain less than 60% of pelagic plus neritic grains and also less than 60% of siliciclastic plus volcanoclastic grains.

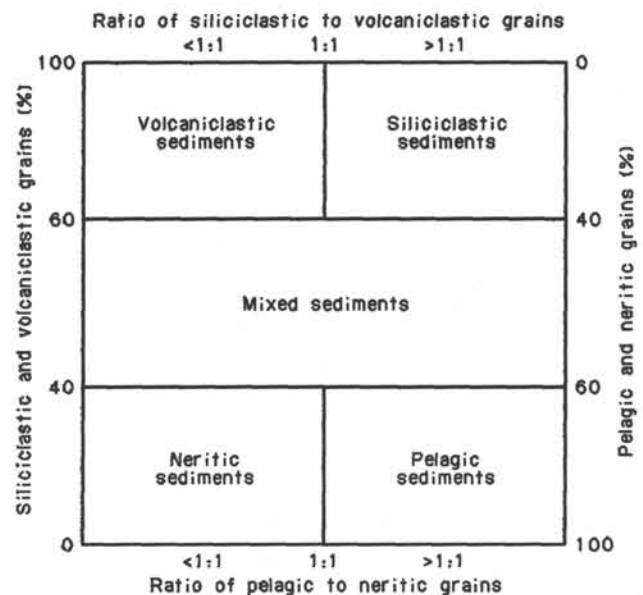


Figure 7. Diagram showing classes of granular sediments.

Classification of Granular Sediment

A granular sediment can be classified by designating a principal name and major and minor modifiers. The principal name of a granular sediment defines its granular-sediment class; the major and minor modifiers describe the texture, composition, fabric, roundness, or other characteristics of the grains themselves (Table 1).

Principal Names

Each granular-sediment class has a unique set of principal names: for pelagic sediment, the principal name describes the composition and degree of consolidation using the following terms:

1. Ooze: unconsolidated calcareous and/or siliceous pelagic sediment.

2. Chalk: firm pelagic sediment composed predominantly of calcareous grains.

3. Limestone: hard pelagic sediment composed predominantly of calcareous grains.

4. Radiolarite, diatomite, spiculite: firm pelagic sediment composed predominantly of siliceous radiolarians, diatoms, and sponge spicules, respectively.

5. Chert: hard pelagic sediment composed predominantly of siliceous grains.

Table 1. Outline of granular-sediment classification scheme.

Sediment class	Major modifiers	Principal names	Minor modifiers		
Pelagic sediment	Composition of pelagic and neritic grains present in major amounts	Ooze	Composition of pelagic and neritic grains present in minor amounts		
		Chalk			
	Texture of clastic grains present in major amounts	Limestone	Texture of clastic grains present in minor amounts		
		Radiolarite			
		Diatomite			
Neritic sediment	Composition of neritic and pelagic grains present in major amounts	Boundstone	Composition of neritic and pelagic grains present in minor amounts		
		Grainstone			
	Texture of clastic grains present in major amounts	Packstone	Texture of clastic grains present in minor amounts		
		Wackestone			
Siliciclastic sediment	Composition of all grains present in major amounts	Gravel	Composition of all grains present in minor amounts		
		Sand			
	Grain fabric (gravels only)	Silt	Texture and composition of siliciclastic grains present as matrix (for coarse-grained clastic sediments)		
		Clay (etc.)			
	Grain shape (optional)	Clay (etc.)	Clay (etc.)	Clay (etc.)	
					Sediment color (optional)
	Volcaniclastic sediment	Composition of all volcaniclasts present in major amounts	Breccia	Composition of all volcaniclasts present in minor amounts	
			Lapilli		
		Composition of all pelagic and neritic grains present in major amounts	Ash/tuff	Composition of all neritic and pelagic grains present in minor amounts	
			Ash/tuff		
Texture of siliciclastic grains present in major amounts		Ash/tuff	Composition of all neritic and pelagic grains present in minor amounts	Composition of all neritic and pelagic grains present in minor amounts	
					Ash/tuff
Mixed sediment		Composition of neritic and pelagic grains present in major amounts	Mixed sediment	Composition of neritic and pelagic grains present in minor amounts	
					Mixed sediment
		Texture of clastic grains present in major amounts	Mixed sediment	Composition of neritic and pelagic grains present in minor amounts	Texture of clastic grains present in minor amounts
	Mixed sediment				

6. Conglomerate: the term "conglomerate," defined below under siliciclastic sediments, is introduced to the ODP classification for textural conglomerates composed primarily of resedimented calcareous pelagic material. These sediments would otherwise be classified as oozes.

Very few neritic sediments were cored during Leg 123, and they are not described further here. Refer to the Leg 122 "Explanatory Notes" chapter (Shipboard Scientific Party, 1989) for classification of neritic sediments. For siliciclastic sediment, the principal name describes the texture and is assigned according to the following guidelines:

1. The Udden-Wentworth grain-size scale (Wentworth, 1922; Table 2) defines the grain-size ranges and the names of the textural groups (gravel, sand, silt, clay) and subgroups (e.g., fine sand, coarse silt) that are used as the principal names of siliciclastic sediment.

2. When two or more textural groups or subgroups are present in a siliciclastic sediment, they are listed as principal names in order of increasing abundance (Fig. 8; Shepard, 1954).

3. The suffix "-stone" can be affixed to the principal names sand, silt, and clay when the sediment is lithified; shale can be

Table 2. Udden-Wentworth grain-size scale for siliciclastic sediments (Wentworth, 1922).

Grain size		Phi (ϕ)	Wentworth size class
(mm)	(μ m)		
		20	
4096		12	Boulder (-8 to -12 ϕ)
1024		10	
256		8	Cobble (-6 to -8 ϕ)
64		6	
16		4	Pebble (-2 to -6 ϕ)
4		2	
3.36		1.75	Granule
2.83		1.15	
2.38		1.25	
2.00		1.0	Very coarse sand
1.68		0.75	
1.41		0.5	Coarse sand
1.19		0.25	
1.00		0.0	Medium sand
0.84		0.25	
0.71		0.5	Fine sand
0.59		0.75	
1/2	500	1.0	Very fine sand
0.42	420	1.25	
0.35	350	1.5	Coarse silt
0.30	300	1.75	
1/4	250	2.0	Medium silt
0.210	210	2.25	
0.177	177	2.5	Fine silt
0.149	149	2.75	
1/8	125	3.0	Very fine silt
0.105	105	3.25	
0.088	88	3.5	Coarse silt
0.074	74	3.75	
1/16	63	4.0	Medium silt
0.063	53	4.25	
0.044	44	4.5	Fine silt
0.037	37	4.75	
1/32	31	5.0	Very fine silt
1/64	15.6	6.0	
1/128	7.8	7.0	Clay
1/256	3.9	8.0	
	2.0	9.0	Clay
	0.00098	10.0	
	0.00049	11.0	
	0.00024	12.0	
	0.00012	13.0	
	0.00006	14.0	

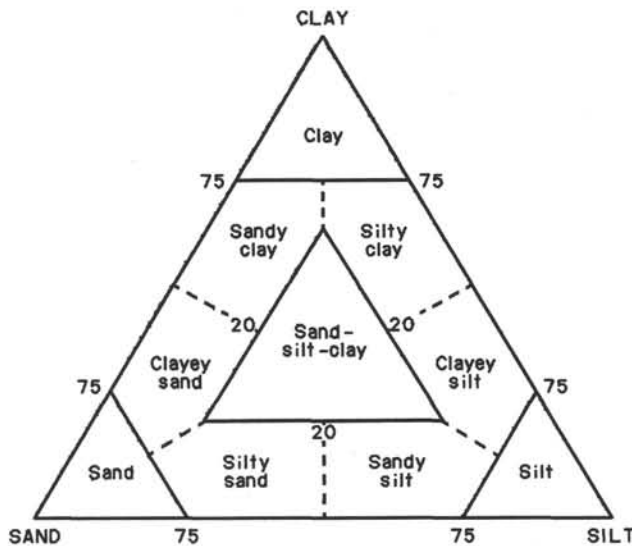


Figure 8. Ternary diagram showing principal names for siliciclastic sediments (from Shepard, 1954).

used as a principal name for a lithified and fissile siltstone or claystone. Conglomerate and breccia are used as principal names of gravels with well-rounded and angular clasts, respectively. These can be either grain- or matrix-supported.

For volcanoclastic sediment, the principal name describes the texture. The names and ranges of three textural groups (from Fisher and Schmincke, 1984) are as follows:

1. Volcanic breccia: pyroclasts greater than 64 mm diameter.
2. Volcanic lapilli: pyroclasts 2 to 64 mm diameter.
3. Volcanic ash: pyroclasts less than 2 mm diameter. When lithified, these are tuffs. Only volcanic ash was encountered during Leg 123.
4. Clastic sediments of volcanic provenance are described in the same fashion as siliciclastic sediments, noting the dominant composition of volcanic grains.

For mixed sedimentary deposits, the principal name describes the degree of consolidation; they are either mixed sediments, or mixed sedimentary rocks.

Major and Minor Modifiers

The principal name of a granular sediment is preceded by major modifiers and followed by minor modifiers (preceded by the suffix 'with') that describe the lithology of the sediment in greater detail (Table 1). The most common uses of major and minor modifiers are to describe the compositions and textures of grain types that are present in major (greater than or equal to 25%) and minor (10%–24.9%) proportions. In addition, major modifiers can be used to describe grain fabric and shape, as well as sediment color. Nomenclature for major and minor modifiers is outlined below.

The composition of pelagic grains can be described with the major and minor modifiers diatom(-aceous), radiolarian, spicules(-ar), siliceous, nannofossil, foraminifer(-al), and calcareous, for example. The terms "siliceous fragment" and "calcareous fragment" are used to describe siliceous or calcareous pelagic grains of uncertain origins.

The textures of siliciclastic sediments are described by the major and minor modifiers gravel, sand, silt, and clay. The compositions of siliciclastic grains can be described by:

1. Mineralogy: using modifiers such as "quartz," "feldspar," "glaucinite," "zeolitic," "lithic" (for rock fragments), "calcareous," or "sapropelic" (for detrital clasts of calcium carbonate and organic matter, respectively); and
2. Provenance: the source of rock fragments (particularly in gravels, conglomerates, and breccias) can be described by modifiers such as volcanic, sed-lithic, meta-lithic, gneissic, basaltic, etc.

The composition of volcanoclastic grains is described by the major and minor modifiers lithic (rock fragments), vitric (glass and pumice), and crystal (mineral crystals), or by modifiers that describe the compositions of the liths and crystals (e.g., rhyolitic or feldspar).

The fabric of the sediment can be described by the major modifiers grain-supported, matrix-supported, and imbricated. Generally, fabric descriptors are applied only to gravels, conglomerates, and breccias, for they provide useful information about their transport history.

The shapes of grains are described as rounded, subrounded, subangular, and angular.

Sediment color is determined by comparison with Munsell Soil Color Charts (1975), and can be used as a major modifier.

Chemical Sediments

Classes of Chemical Sediment

Chemical sediments are composed of minerals that formed by inorganic processes such as precipitation from solution or colloidal suspension, deposition of insoluble precipitates, or recrystallization of detrital evaporites and siliceous, calcareous, or carbonaceous biogenic debris. They commonly have a crystalline texture. Five classes of chemical sediments are: carbonaceous sediments, evaporites, silicates, carbonates, and metalliferous sediments.

Carbonaceous sediments are composed of greater than 50% organic remains, principally plant and algal remains, that have been altered by carbonization, bituminization, or putrefaction from their original form. The only carbonaceous sediments found during Leg 123 are coals. These are thin and rare, and are not ranked, but are simply listed as "coal."

Evaporites were not encountered during Leg 123.

Silicates and carbonates are sedimentary rocks that are non-granular and nonbiogenic and are composed of silicate and carbonate minerals. Silicates and carbonates may have formed from the recrystallization of siliceous and calcareous grains, but are distinguished by the absence of clearly identifiable granular or biogenic components. They may also form as primary precipitates, as in the case of some dolomites, or as hydrothermal alteration products, such as zeolites. They are classified according to their mineralogy, using principal names such as chert (microcrystalline quartz), calcite, dolomite, and zeolite. They are modified as crystalline, microcrystalline, massive, or amorphous. The name "rhodochrosite" is applied to a sediment or rock whose dominant constituent consists of (commonly) silt-sized nodules of a carbonate that has been identified as rhodochrosite, dolomite, or as a mixture of rhodochrosite and dolomite.

Metalliferous sediments are nongranular, nonbiogenic sedimentary rocks that include pyrite, goethite, manganite, and other metal-bearing minerals. They are classified according to their

mineralogy. Metalliferous sediments are extremely uncommon in cores from Leg 123.

Sediment Measurements

Grain Size

For routine assignment of sediments to textural classes, grain sizes were estimated visually from core material, smear slides, and thin sections.

X-Ray Diffraction

X-ray diffractograms were used to determine bulk mineralogy, and to identify unusual minerals that were abundant in some of the sediments cored (e.g., rhodochrosite). Some XRD analyses provided qualitative information about the distribution of carbonate in clay-dominated sediments, and of clay in carbonate-dominated sediments. XRD methods are described in the "XRD Analyses" section of this chapter.

X-Ray Fluorescence

XRF data were used to study the elemental variations throughout and within the sediment lithologies, to assess the geochemistry for specific unusual lithologies (i.e., bentonite, ash layers), and to identify subtle stratigraphic trends in mineral chemistry. XRF methods are described in the "XRF Analyses" section of this chapter.

Calcium Carbonate

Calcium carbonate analyses derived from headspace sample squeeze cakes were too widely spaced to characterize the observed cyclicity in carbonate content within the recovered sediments. Further, many headspace samples were taken from intervals contaminated by caved pebbles or consisting of several amalgamated lithologies. These were therefore supplemented with carbonate bomb analyses, according to a dual sampling scheme. Part I of this sampling program consisted of bomb analyses systematically placed within observably different portions of repetitive sequences. In Part II of the sampling program red, green, brown, and black clays and claystones, and red, pink, pale green, gray, and brown calcareous oozes and chalks and clayey calcareous oozes and chalks were sampled to evaluate visual and acid-test estimates of carbonate content to calibrate barrel sheet summaries.

Reliability of Smear Slide Data

An experiment was conducted to evaluate the relationship between CaCO_3 content estimated from smear slides and measured with a carbonate bomb (Fig. 9). The purpose was to evaluate the reliability of quantitative estimates of components in smear slide descriptions.

Twenty-one smear slides were compared to carbonate bomb analyses. These were chosen as follows. The smear slides and corresponding carbonate bomb samples were taken from the same sedimentation units, and there was no observable lithologic boundary between paired samples. For example, two samples from a homogeneous interval of nannofossil ooze within a single graded carbonate sequence would be compared, but samples taken from successive (apparently identical) graded sequences would not. Likewise, if a distinct color change or significant observable grain-size change occurred between a pair of potential samples, then they were rejected from the analysis.

Smear slide estimates of carbonate content are consistently higher than bomb measurements. All but two smear-slide estimates are between 12% below and 46% above the carbonate bomb values for carbonate content; most smear-slide estimates exceed bomb estimates by less than 35%. Deviation of smear-slide estimates from bomb estimates is greatest at intermediate values of carbonate content.

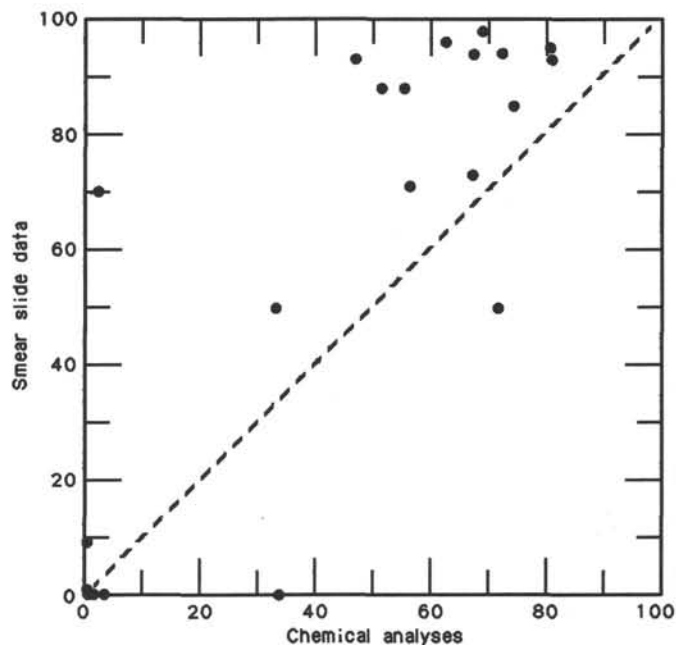


Figure 9. Graph of calcium carbonate content (%) estimated from smear slides vs. calcium carbonate content (%) measured by carbonate bomb analyses. Paired samples were collected from a single, homogeneous interval of sediment or rock (N = 21).

There are no readily available objective measurements of the percentages of other components estimated in smear-slide descriptions, but some general conclusions may be drawn from the carbonate-content data and from other observations made during core description.

1. Smear-slide component percentages should not be regarded as *quantitative*.
2. Smear-slide component percentages do, however, give accurate *qualitative* information about component abundances.
3. Highly visible components (benthic foraminifers, discoasters) are consistently overestimated, whereas components that are difficult to see (clay) are underestimated.
4. We also observed that the percentages of extremely large (coarser than fine sand-sized) particles are underestimated. This is partly because they tend to wash to the edges of the smear slides.

Cretaceous-Pleistocene Turbidite Sequences

The majority of sediments cored at Sites 765 and 766 are graded carbonate sequences composed of redeposited pelagic grains, although red and green claystones, more typical of the sedimentary cover of abyssal plains, were also found. The classification scheme and graphic conventions commonly used by ODP sedimentologists for pelagic carbonate sediments largely ignore textural parameters, which are important to the description of redeposited sediments. Accordingly, features were added to the standard procedures to maximize the utility of the result, while minimizing changes in the standard procedures and classification.

Effect on Classification

The repetitive sequences found at Site 765 consist largely of resedimented pelagic grains that were deposited initially as pelagic sediments and that were later redeposited in a pelagic setting (the Argo Abyssal Plain). Therefore, they are classified as pelagic sediments according to the ODP classification, even though they are graded event deposits.

One feature was modified in the classification. Several Tertiary units consist of matrix-supported bimodal sediments in which the matrix consists of clay-to sand-sized pelagic carbonate grains, and the larger clasts consist of pebbles. Most pebble lithologies closely resemble host lithologies, but exotic pebbles (commonly volcanic) occur in several of these units and predominate in one. These sediments are classified as conglomerates by analogy with siliciclastic conglomerates of similar textures.

Effect on Barrel Sheets

Barrel sheets are the primary source of sedimentologic information in ODP reports, and therefore it is important that they accurately represent the nature of the sediments. The grain-size characteristics and sedimentary structures of graded calcareous sequences, such as those that make up most of the sediments cored during Leg 123, are critical to the interpretation of the depositional conditions of these sediments. Therefore, we employ four conventions that maximize the utility of barrel sheet descriptions of these units.

1. Graded intervals down to about 10 cm thick are shown as fining-upward cycles in the sedimentary structures column. Even thinner sequences, or discrete graded intervals within larger-scale graded intervals, are indicated as horizontal dotted lines.

2. The sediment names of graded sequences in barrel-sheet text summaries are followed, in parentheses, by brief descriptions of their grain-size characteristics where appropriate (e.g., "sequences typically fine-sand sized and foraminifer-dominated at the base to clay-sized and nannofossil-dominated at the top").

3. Barrel-sheet text summaries include explicit mention of sedimentary structures observed in graded sequences. Most "graded sequences" described in barrel-sheet text summaries are believed to have formed as turbidites.

Finally, new symbols for sedimentary structures are introduced (Fig. 5), and graphic lithologic symbols used on barrel sheets are modified slightly from Leg 122 usage (Fig. 4).

BIOSTRATIGRAPHY

Time Scales

The chronostratigraphy used for the Cenozoic follows Berggren et al. (1985a, 1985b), with minor modifications to the age of stage boundaries and zonal correlation based on new data by Zijdeveld et al. (1986) and Aubry et al. (1988; see Figs. 10, and 11). For the Mesozoic, the chronostratigraphic nomenclature and geochronology of Kent and Gradstein (1985) were used. Both time scales use high-temperature radiometric dates, rather than low-temperature dates or a mixture of both for absolute dating (Gradstein et al., 1988). Beyond the argument of the relative merits of high- vs. low-temperature dates, all numerical time scales are hindered by a lack of direct dates for most of the chronostratigraphic boundaries. The interpolation scheme used by the authors quoted was based upon construction of a standard magnetochronology from comparison of seafloor marine magnetic-anomaly spacing in different ocean basins. Calibration is through magnetobiostratigraphy in sedimentary sections and from isochrons of the ocean crust.

We have updated the Mesozoic scale slightly using new correlations of Lower Cretaceous stage boundaries and magnetostratigraphy (Fig. 12 (backpocket figure)). These modifications are based on Ogg (1984), Ogg and Lowrie (1986), Bralower (1987), and Ogg and Steiner (in press). The following correlations are used:

Barremian/Aptian boundary, slightly below M0R (119 Ma).
Hauterivian/Barremian boundary, within M5 to M7 (127 Ma).

Valanginian/Hauterivian boundary, within or near M10R (131.5 Ma).

Berriasian/Valanginian boundary, in the middle of M15N (138.5 Ma).

Tithonian/Berriasian boundary, in the middle of M19N, which places it at the boundary of calpionellid Zones A and B (see Remane et al., 1986). This coincides with the base of the combined *Berriasella jacobigrandis* ammonite zone (approximately 145 Ma).

The precision of our interpolations far exceeds the temporal accuracy.

Biostratigraphy

Calcareous Nannofossils

Cenozoic calcareous nannofossil zonation applied during Leg 123 included Gartner (1977) for the Pleistocene and the zonation of Martini (1971), Okada and Bukry (1980), and Bukry (1981) for the remainder of the Cenozoic. All zonation were reasonably applicable to the eastern Indian Ocean and, where usable, Okada and Bukry's zonation (1980) was preferred over Martini's zonation (1971) because of its higher resolution.

The zonation of Thierstein (1971, 1976), Sissingh (1977), Roth (1978), as well as unpublished data, were used to correlate Cretaceous sedimentary strata. The small amount of nannofossil research in the Jurassic period has thus far precluded the development of a stable, satisfactory, or widely accepted zonal scheme. In addition, Jurassic nannofossil data from extra-European areas have indicated the presence of provincialism. Jurassic nannofossils from Leg 123 were biostratigraphically zoned using available information from the East Indian Ocean region, together with limited application of zonation schemes developed predominantly in the northwest European area. For the Middle Jurassic to Lowermost Cretaceous interval, data from DSDP Leg 27, Site 261 were used and include those of Proto Decima (1974) and Cooper (1984). Other zonal schemes employed include Thierstein (1976), Roth et al. (1983), Bralower (1987), and Bown et al. (1988). In the Triassic and Lower Jurassic, data from Bown (1987), Bown et al. (1988), and Bown and Lord (in press) were used.

Planktonic Foraminifers

Neogene

The tropical zonation of Blow (1969), as amended by Kennett and Srinivasan (1983), was followed for this sequence. The boundary between Zones "N19" and "N20" was taken at the first appearance of *Globorotalia crassaformis*. The first appearance of *Sphaeroidinella dehiscens* may be diachronous in the Indian Ocean (Vincent, 1977) and may be unsuitable for marking the boundary between Zones N18 and N19. This level is approximately coincident with the first appearance of *Globorotalia (Hirsutella) margaritae*, as defined by Kennett and Srinivasan (1983), and the extinction of *Globorotalia (Globorotalia) plesiotumida*. The N-zonation has been used extensively on the Australian Northwest Shelf adjacent the Argo Abyssal Plain (Apthorpe, 1988; Chaproniere, 1981) and elsewhere in the Indian Ocean (Vincent, 1977).

Paleogene

The tropical zonation of Blow (1969, 1979) was applied to the upper Eocene-Oligocene section, and Berggren's zonation (1969) was used for the Paleocene-middle Eocene. A similar zonal scheme was employed for the Wombat Plateau succession drilled during Leg 122 (Shipboard Scientific Party, 1989), and by McGowran (1977) for Deep Sea Drilling Project sites in the northern and eastern Indian Ocean. Apthorpe (1988) applied a

Geochronometric scale (Ma)	Marine magnetic anomaly	Polarity	Chron.	Standard epoch	Calcareous nannofossils		Planktonic foraminifers	Radiolarians	
					Okada & Bukry (1980)	Martini (1971)			
1	1	Normal	B.	C1	Pleistocene	CN15 CN14b	NN21 NN20	N23	<i>Lamprocyrtis haysi</i>
1	1	Normal	Matuyama			CN14a	NN19	N22	<i>Pterocanium prismatium</i>
2	2	Reversed	Matuyama	C2	late Pliocene	CN13a CN13b	NN18	N21	
2	2	Reversed	Gauss			CN12d CN12b	CN12c		NN17
3	3	Normal	Gauss	C2a	early Pliocene	CN12a	NN16	"N20"	<i>Stichocorys peregrina</i>
3	3	Normal	Gilbert	C3	early Pliocene	CN11a CN11b	NN15		
4	4	Reversed	Gilbert	C3	early Pliocene	CN10c	NN14	"N19"	<i>Stichocorys peregrina</i>
4	4	Reversed	5			C3a	CN10b		
5	5	Normal	5	C3a	late Pliocene	CN10a	NN11	N18	<i>Didymocyrtis penultima</i>
5	5	Normal	6	C3a		CN9b	NN10	N17b	
6	6	Reversed	6	C4	late Pliocene	CN9a	NN11	N17a	<i>Didymocyrtis antepenultima</i>
6	6	Reversed	7						
7	7	Normal	7	C4a	late Pliocene	CN8b CN8a	NN10	N16	<i>Didymocyrtis antepenultima</i>
7	7	Normal	8						
8	8	Reversed	8	C4a	late Pliocene	CN7a+b	NN9	N16	<i>Didymocyrtis antepenultima</i>
8	8	Reversed	9						
9	9	Normal	9	C5	middle Miocene	CN6	NN8	N15	<i>Diartus petterssoni</i>
9	9	Normal	10						
10	10	Reversed	10	C5	middle Miocene	CN5b	NN7	N14	<i>Diartus petterssoni</i>
10	10	Reversed	11						
11	11	Normal	11	C5a	middle Miocene	CN5a	NN6	N13	<i>Diartus petterssoni</i>
11	11	Normal	12						
12	12	Reversed	12	C5a	middle Miocene	C5a	NN6	N12	<i>Diartus petterssoni</i>
12	12	Reversed	13						
13	13	Normal	13	C5a	middle Miocene	C5a	NN6	N11	<i>Diartus petterssoni</i>
13	13	Normal	14						
14	14	Reversed	14	C5b	middle Miocene	CN4	NN5	N10	<i>Dorcadospyrus alata</i>
14	14	Reversed	15						
15	15	Normal	15	C5b	middle Miocene	CN4	NN5	N9	<i>Dorcadospyrus alata</i>
15	15	Normal	16						
16	16	Reversed	16	C5c	early Miocene	CN3	NN4	N8	<i>Calocyrtella costata</i>
16	16	Reversed	17						
17	17	Normal	17	C5c	early Miocene	CN3	NN4	N7	<i>Calocyrtella costata</i>
17	17	Normal	18						
18	18	Reversed	18	C5d	early Miocene	CN2	NN3	N6	<i>Stichocorys wolffii</i>
18	18	Reversed	19						
19	19	Normal	19	C5e	early Miocene	CN2	NN3	N5	<i>Stichocorys delmontensis</i>
19	19	Normal	20						
20	20	Reversed	20	C6	early Miocene	CN1	C	N4b	<i>Cyrtocapsella tetrapera</i>
20	20	Reversed	21						
21	21	Normal	21	C6a	early Miocene	CN1	C	N4b	<i>Cyrtocapsella tetrapera</i>
21	21	Normal	22						
22	22	Reversed	22	C6aa	early Miocene	CN1	C	N4b	<i>Cyrtocapsella tetrapera</i>
22	22	Reversed	23						
23	23	Normal	23	C6b	early Miocene	CN1	a+b	NN1	<i>Lychnocanoma elongata</i>

Figure 10. Correlation of Neogene chronostratigraphy, biostratigraphy, and magnetostratigraphy used during Leg 123. Note: (1) revised age of the Miocene/Pliocene boundary was taken from Zijdeveld et al. (1986); (2) correlation of Pliocene-Pleistocene radiolarian zones to magnetostratigraphy follows Sanfilippo et al. (1985); correlation of Miocene radiolarian zones follows Berggren et al. (1985b); (3) magnetic chron terminology follows that adopted by Leg 108 (Ruddiman, Sarnthein, et al., 1988); (4) interpolated ages of magnetic polarity reversals and planktonic foraminiferal/nannofossil datums used to define zones are after Berggren et al. (1985b); (5) planktonic foraminiferal "N" zonation slightly modified after Kennett and Srinivasan (1983). Zone N17 is subdivided into two parts using the FO of *Pulleniatina primalis*; Zone N4B subdivided on the FO of *Globoquadrina dehiscens*; the base of Zone N13 is defined by the LO of *Globorotalia fohsi* lineage; the base of N20 is defined here as the FO of *Globorotalia crassaformis* s.l. at 4.3 Ma.

Geochrono- metric scale (Ma)	Marine magnetic anomaly	Polarity	Chron.	Standard epoch	Calcareous nannofossils		Planktonic foraminifers Blow (1969) Berggren (1969)	Radiolarians Sanfilippo et al. (1985)			
					Okada & Bukry (1980)	Martini (1971)					
24	6C		C6c	late Oligocene	CP19b	NP25	N4a	<i>Dorcadospyrus ateuchus</i>			
26	7		C7								
	7A		C7a								
28	8		C8								
	9		C9	early Oligocene	CP19a	NP24	P21a	----- <i>Theocyrtis tuberosa</i> -----			
30	10		C10								
32	11		C11								
	12		C12								
34				CP17	NP22	P19	----- <i>Cryptopora ornata</i> -----				
				CP16c							
36	13		C13	CP16b				NP21	P18		
				CP16a	NP19/20	P17	----- <i>Calocyclus bandyca</i> -----				
38	15		C15	CP15b							
	16		C16	late Eocene	CP15a	NP18	P16	----- <i>Carpocanistrum azyx</i> -----			
40	17		C17								
42	18		C18								
	19		C19								
44				middle Eocene	CP14a	NP16	P12	<i>Podocyrtis ampla</i> ----- -----			
46	20		C20								
							CP13c		NP15	P11	
48							CP13b				
	21		C21	CP13a							
50				early Eocene	CP12b	NP14	P10	<i>Dictyoprora mongolfieri</i> ----- <i>Theocotyle cryptocephala</i> ----- <i>Phormocyrtis striata</i> -----			
52	22		C22								
							CP12a		NP13	P9	
							CP11		NP12	P8	
54	23		C23	late Paleocene	CP10	NP11	P7	<i>Buryella clinata</i> ----- <i>Bekoma bidartensis</i> -----			
56	24		C24								
							CP9b		NP10	P6b	
							CP9a		NP9	P6a	
58				early Paleocene	CP8b	NP8	P5	----- <i>Unzoned</i> -----			
	25		C25								
							CP8a		NP7	P4	
60	26		C26								
				early Paleocene	CP7	NP6	P3b	----- <i>Unzoned</i> -----			
									CP6	NP5	P3a
62									CP5	NP4	P2
	27		C27								
64	28		C28	early Paleocene	CP2	NP3	P1d	----- <i>Unzoned</i> -----			
	29		C29								
66				CP1b	NP2	P1c					
				CP1a	NP1	P1c+a+b					

Figure 11. Correlation of Paleogene chronostratigraphy, biostratigraphy, and magnetostratigraphy used during Leg 123. Revised age of Paleocene/Eocene boundary is after Aubry et al. (1988). Correlation of radiolarian zones (Sanfilippo et al., 1985) follow correlation to nannofossil zones of Berggren et al. (1985a).

somewhat different (unpublished) zonation on the Australian Northwest Shelf.

Jurassic to Cretaceous

Caron's zonation (1985) was used for the Aptian-Maestrichtian section. As many index species appear to be missing from the low-diversity assemblages recovered from this section, most of the zonal assignments were broad. Planktonic assemblages recorded elsewhere from the northwestern Australian margin also lack many of the zonal index forms (Belford, 1981; Herb and Scheibnerova, 1977; McGowran, 1977; Wright and Apthorpe, 1976). The scattered Early Cretaceous planktonic foraminifers encountered during Leg 123 were zoned following Stam (1986), but most have not been documented from the Indian Ocean realm. These primitive planktonic foraminifers may occur in bathyal marine strata within the region.

Benthic Foraminifers

The Cenozoic biostratigraphy of calcareous benthic foraminifers recovered during Leg 123 was compared with the biostratigraphic ranges of Tjalsma and Lohmann (1983) and Van Morkhoven et al. (1986). These zonal schemes were applicable at Site 766, but because of the location of Site 765 beneath the carbonate compensation depth (CCD), this biostratigraphy was used mainly in turbidites.

The Upper Cretaceous zeolitic clays in DSDP Site 261 on the Argo Abyssal Plain contain a distinct assemblage of small agglutinated benthic foraminifers (Krashennikov, 1974). Leg 123 biostratigraphy of these taxa, some of which may be unique to the abyssal realm, was based on the zonation of Geroch and Nowak (1984). Their zonation is based on similar assemblages from the flysch units of the Polish Carpathians and has been used successfully for Upper Cretaceous abyssal red clay sediments from DSDP Site 603 and ODP Site 641 in the North Atlantic (Moullade et al., 1988). The taxonomy and biostratigraphy of Upper Cretaceous calcareous benthic foraminifers recovered during Leg 123 follows Sliter (1977) and Dailey (1983). For the Lower Cretaceous, Gradstein (1978), Sliter (1980), and Moullade (1984) illustrated calcareous and agglutinated benthic taxa found in Atlantic abyssal sediments, and their biostratigraphical schemes were used at Leg 123 sites.

The Neocomian abyssal benthic foraminifers of Leg 123 were dated using the taxonomy and biostratigraphy of Bartenstein and Brand (1951), Kuznetsova (1974), Gradstein (1983, 1986), Sliter (1980), Hart (1984), and Williamson and Stam (1988). In the literature, comparison of the Argo Abyssal Plain benthic record in DSDP Site 261 with that of Atlantic DSDP Sites 534 and 105 revealed close agreement in taxa observed, which leads us to postulate comparable stratigraphic ranges.

Radiolarians

Cenozoic

The Cenozoic radiolarian assemblages were assigned to biozones initially proposed by Riedel and Sanfilippo (1978), and later reviewed by Sanfilippo et al. (1985). The late Neogene correlation of radiolarian datums to magnetostratigraphy by Casey and Reynolds (1980) proved useful.

Mesozoic

At present, no standard radiolarian zonation is available for the Cretaceous. Ages were based on an integration of radiolarian ranges proposed by Sanfilippo and Riedel (1985), Schaff (1981, 1985), Pessagno (1977), and Aita (1987). The Lowermost Cretaceous was zoned after Baumgartner (1984, 1987).

Palynomorphs

Dinoflagellates

There is no widely accepted Southern Hemisphere or tropical Cenozoic dinoflagellate zonation, but one of the more applicable ones is that of Williams (1977). Hansen (1977) produced a detailed Maastrichtian/Danian boundary zonation that can be applied with success to the northwestern Australian margin (McMinn, 1988a). Helby et al. (1987) produced a comprehensive Australian Mesozoic dinoflagellate zonation that covers the Jurassic to Late Cretaceous assemblages. However, the most applicable Upper Cretaceous zonation was that of McMinn (1988b), which was developed on material from the northwestern Australian margin.

Spores and Pollen

The only Cenozoic spore and pollen zonations developed in Australia were produced on the southern margin. Because of strong climatic control on such zonations during this time, they are of questionable value on the northwestern margin. A Mesozoic zonation for spore and pollen is included in Helby et al. (1987), and all Mesozoic assemblages have been correlated with this biostratigraphic framework.

Methods and Procedures

Calcareous Nannofossils

Nannofossil samples for biostratigraphic examination were prepared by making simple smear slides from raw sediment samples. Smear slides were preferred instead of gravity settling because of a possible tendency for the latter process to exclude smaller specimens. Preferential concentration of relatively complete and well-preserved nannofossil assemblages in the upper part of turbidite sections made it necessary to obtain smear slides from these sediments for accurate dating (see "Biostratigraphy" section, Site 765 chapter, this volume).

Estimates of the relative abundance of calcareous nannofossils in the Cenozoic, where they usually constitute a sizable fraction of the sediment, were determined following these guidelines:

VA (Very Abundant)	> 20 specimens/field of view
A (Abundant)	> 10 specimens/field of view
C (Common)	1-10 specimens/field of view
F (Few)	1 specimen/2-10 fields of view
R (Rare)	1 specimen/11-100 fields of view
VR (Very Rare)	1 specimen/> 100 fields of view

All estimates were made at a magnification of 1250X.

Samples in which nannofossils composed a smaller fraction of the total sediment, particularly in the Mesozoic, required a different scale for estimating relative abundance:

A (Abundant)	> 100 specimens observed
C (Common)	1-10 specimens observed
F (Few)	3-10 specimens observed
R (Rare)	1-2 specimens observed

These abundances were estimated after two transverse of a slide at a magnification of 1250X.

The average preservation state of all nannofossil taxa was estimated for each slide. An average is necessary as certain species are more susceptible to overgrowth and/or dissolution than others. Letters representing preservation states were designated as follows:

- E (Excellent) - No evidence of any overgrowth/dissolution on any specimens.
 G (Good) - Only slight overgrowth/dissolution of most specimens.
 M (Moderate) - Most specimens display modest degrees of overgrowth/dissolution; species identification not impaired.
 P (Poor) - Most specimens display significant amounts of overgrowth/dissolution; species identification sometimes impaired.
 VP (Very Poor) - All specimens display profound overgrowth/dissolution; species identification impossible.

Foraminifers

Carbonate-sand samples were disaggregated in boiling water with added detergent and Calgon; the claystone samples were disaggregated in a weak solution of hydrogen peroxide and Calgon. The residues were washed on a 63- μ m sieve and dried under a heat lamp. The sand-sized sediment fraction was examined under a stereo microscope, and an assemblage of planktonic foraminifers was picked selectively from each productive sample and mounted on a micropaleontological slide.

The relative abundance of species in an assemblage is based on a visual estimate of the >63- μ m sediment fraction. The following letters are used to indicate abundance:

- A = Abundant (>30%)
 C = Common (15%-30%)
 F = Few (3%-15%)
 R = Rare (<3%)

The state of preservation of planktonic foraminifers is described as follows:

- G - Good (little fragmentation or etching of specimens)
 M - Moderate (fragmentation and etching obvious; or moderate sparry calcite crusts cover specimens)
 P - Poor (most specimens broken and severely corroded; or specimens covered by thick sparry calcite crusts).

Radiolarians

All samples were selected by visual examination of the core with a hand lens or a binocular microscope, which allowed an estimate of abundance and general preservation of radiolarians in the core. In the claystone sequences of Site 765 most radiolarian samples were taken in sandy laminae and layers that showed the least detrital content.

All samples recovered during Leg 123 were crushed into millimeter-sized pieces and then boiled in a mixture of hydrogen peroxide and Calgon for 5 to 20 min. Concentrations varied, depending on the degree of induration of the sediment. Lime-rich samples were first decalcified in 20% hydrochloric acid (HCl). The sample then was sieved and the fraction >44 μ m was analyzed. Some heavily silicified samples would not disaggregate with this process and needed to be digested for 24 hr in 5% hydrofluoric acid (HF), then thoroughly washed and sieved.

Cenozoic residues were embedded in Norland Optical Adhesive using standard smear-slide techniques. The skeletons of most Mesozoic radiolarians are recrystallized as quartz or clay minerals, etc., and/or are filled by matrix or cement and thus cannot be examined using standard transmitted-light techniques. These residues were sieved, dried, and examined using reflected-light methods. Abundance of radiolarians given in biostratigraphic sections of the site chapters was based on slides of sieved acid residues, and thus may differ markedly from the lithologic descriptions, which were based on smear-slide data.

Abundance estimates are completely qualitative and were determined on the visual approximation of the total amount of residue per each 10 cm³ of sediment and of the percentage of radiolarian specimens observed in this residue, either per slide or per picking tray.

- A (abundant) - >2 cm³ of residue, >80% radiolarians. Numerical Value = 5
 C (common) - 0.2-2 cm³ of residue, 10%-80% radiolarians. Numerical Value = 4
 F (few) - 0.2-2 cm³ of residue, 1%-10% radiolarians. Numerical Value = 3
 R (rare) - 0.2-2 cm³ of residue, <1% radiolarians. Numerical Value = 2
 VR (very rare) - <0.2 cm³ of residue, or <1‰ (per mil) radiolarians. Numerical Value = 1
 — (barren) - no radiolarians in at least one entire slide or picking tray. Numerical Value = 0

Radiolarian preservation ranges from very poor to very good. Degraded preservation is a result of recrystallization of opaline silica as quartz and of replacement by clay minerals, zeolites, etc. Preservation was defined as follows:

- VG (very good) - majority of specimens observed are complete with spines intact, no overgrowths or recrystallization. Nearly all specimens determinable. Numerical Value = 5
 G (good) - many specimens complete with spines intact, little or no overgrowths, cement or matrix infill occurs, but outer surface intact. Most specimens determinable. Numerical Value = 4
 M (moderate) - a substantial portion of the specimens broken, and some degree of overgrowth, etching or replacement by minerals other than quartz or pyrite. 50% of specimens undeterminable. Numerical Value = 3
 P (poor) - specimens mostly broken and fragmentary or strongly etched or replaced by other minerals. <5% of specimens determinable. Numerical Value = 2
 VP (very poor) - specimens only present as inner molds or ghosts, or fragments. None determinable. Numerical Value = 1
 — (not determinable). Numerical Value = 0

Palynomorphs

The initial method of disaggregation depended on sediment type. Semiconsolidated, noncalcareous sediments were treated with Calgon; calcareous sediments with HCl and then HF; argillaceous sediments with HF. Following disaggregation, the carbonaceous fraction was floated off in a zinc bromide solution (specific gravity, 2.1) and then mounted in glycerin jelly. All Lower Cretaceous samples were first treated with HF. Generally, only core-catcher samples were analyzed, although where the lithology of this sample was inappropriate, a core sample was also processed.

Palynomorph abundance is reported as follows:

- A - abundant (more than 20%)
 C - common (5%-20%)
 F - few (1%-4%)
 R - rare (1% or less)

Palynomorph preservation was reported as follows:

- G - good (more than 75% undamaged specimens, i.e., not oxidized, broken or folded)

M - moderate (25%–75% undamaged specimens)
 P - poor (less than 25% undamaged specimens).

Dinoflagellate and spore-pollen assemblages were treated separately. A relative dinoflagellate abundance is also given. This is the percentage of dinoflagellates in a palynomorph assemblage.

PALEOMAGNETICS

Magnetic Remanence (Archive Halves)

Natural magnetic remanence (NRM) and remanence after alternating field (AF) demagnetization at 5, 10, 15, or 20 milliteslas (mT) were measured using an automated 2G-Enterprises Model 760R long-core cryogenic magnetometer. Readings were made at 5 to 10 cm intervals on nearly every section of the archive core halves.

A new set of AF demagnetization coils had been installed by 2G-Enterprises prior to departure of Leg 123. These coils enabled AF demagnetization in fields of up to 26 mT. However, in keeping with ODP paleomagnetic policy, we rarely applied AF demagnetization fields exceeding the mean destructive field (MDF) for the various sediment types. In general, upon AF demagnetization at 10 mT, characteristic polarity was evident for most Tertiary sediments. Most Mesozoic sediments and basalts were progressively demagnetized at 10 and 15 mT and measured at 5-cm intervals to obtain detailed polarity records. Whenever possible, polarity interpretations are based upon analyses of both inclination and declination shifts during progressive demagnetization.

The cryogenic magnetometer SQUID (superconducting quantum interference devices) sensors measure magnetization over approximately a region 20 cm long, although each axis has a different response curve. These widths of the sensor regions imply that approximately 150 cm³ of core material contributes to the sensor signals and that sharp magnetic transitions are blurred. However, the increased volume of rock within the sensor region allows one to measure accurately the remanence of very weakly magnetized material, despite the relatively high background noise induced by the rolling of the ship. It was possible to obtain reliable remanence directions from sediments having magnetizations of 10⁻⁵ amperes/meter (A/m; = 10⁻⁸ emu/cm³ in cgs units); greater precision was possible when a correction was performed for the magnetization of the sample holder tray.

Routine cryogenic measurements were not performed on archive halves if the section consisted primarily of drilling-disturbed rubble or of sedimentary debris flows having abundant large clasts, or if the section's liner had ruptured and been reinforced with an increased diameter liner that would not fit into the cryogenic access tube.

The SQUID electronics were read in a 1X-scale flux-counting mode for the X and Z axes. A problem with the Y axis counter during drilling at Site 765 required use of a 10X- or 100X-scale without flux-counting; considering the sensor region volumes, the lowered precision was rarely a problem. Calibration of the axes was checked with the Minispin standard. The set of calibration constants originally provided by 2G-Enterprises were reliable for the 1X-scale flux-counting mode. However, as noted by the Leg 121 paleomagnetists, for higher scales, the axes exhibited relative calibration differences of about 4%.

The cryogenic measurements were collected with an IBM-PC compatible with a new interface and software system (modified from Rhode Island's long-core cryogenic system) that seemed to have eliminated some of the problems reported during previous legs.

Bulk Susceptibility Measurements

The magnetic susceptibility of all cores was measured with a Bartington Instruments magnetic susceptibility meter (Model

M.S.1, using a M.S.1/CX 80 mm whole-core sensor loop set at 0.47 kHz). These measurements were collected at 10-cm intervals and proved useful for identifying turbidite intervals and major lithological changes. Magnetic susceptibility indicates down-hole variations in the concentration of magnetic materials.

Discrete Sampling

Oriented samples in 7-cm³ plastic cubes, or as 12-cm³ minicores, were collected from every core. For the Neogene and Paleocene sediments, two cubes were taken from each core (1) to verify the magnetostratigraphy results from the cryogenic magnetometer and (2) to understand the magnetic behavior of the sediments through stepwise demagnetizations. Some of these samples were analyzed on a Molspin magnetometer, with progressive AF demagnetization steps to 10 mT on a Schonstedt GSD-1 AF-demagnetizer. An hysteretic remanent magnetization (ARM) was observed on several of our samples when demagnetized above 10 mT by this particular instrument; thus, higher AF demagnetization steps were performed using the AF coils on the cryogenic long-core magnetometer. It also became evident that the Molspin lacked the sensitivity necessary to measure the typical Neogene carbonate-rich sediment (magnetic intensities less than 10⁻³ A/m).

For deeply buried lithified Mesozoic sediments, one is often unable to derive characteristic directions or polarities from AF demagnetization at fields below 20 mT. We observed that fields up to MDF were inadequate to obtain a clear reversal pattern from the Lower Cretaceous red radiolarian mudstones recovered at Site 765; indeed, AF demagnetization of up to 15 mT was entirely inadequate to obtain any polarity information in the Lowest Cretaceous reddish mudstones. In addition, when rotated adjacent blocks were within the sense regions, the long-core cryogenic magnetometer yielded inclinations that were too steep.

To obtain the magnetostratigraphy and paleolatitudes from Mesozoic sediments and to study the magnetic properties of the various lithologies, three to five minicores were collected from each section. The shipboard Molspin magnetometer lacked adequate magnetic shielding and sensitivity for studies of weakly magnetized or susceptible sediments. As noted previously, the shipboard cryogenic magnetometer has a problem with excessive noise during ship heave. In addition, thermally demagnetized samples would be exposed to the ambient field before measurement in either magnetometer. Therefore, progressive demagnetizations by thermal or AF treatments with analyses on cryogenic magnetometers were performed within magnetically shielded spaces at shore-based paleomagnetism laboratories.

Basalt samples were collected as oriented minicores and partially analyzed for polarity and paleolatitude using the Molspin magnetometer on board the ship. Additional shore-based studies were made of magnetic mineral composition and magnetic properties.

ORGANIC GEOCHEMISTRY

The organic geochemistry program for Leg 123 included (1) determinations of total carbon and inorganic and organic carbon concentrations by coulometry, (2) determination of total organic carbon concentrations and characterization of organic matter by Rock-Eval pyrolysis, and (3) analyses of permanent and hydrocarbon gases by gas chromatography. Laboratory and analytical procedures are outlined below. Detailed procedures were described by Emeis and Kvenvolden (1986).

Inorganic and Organic Carbon

Analyses of percentages of carbonate carbon and organic carbon were conducted on freeze-dried bulk samples using Coulometrics 5010 coulometers that were coupled either with the 5030 Carbonate Carbon or the 5020 Total Carbon analyzers, respectively. Gases were measured in headspace samples taken

from near organic-geochemistry and interstitial-water samples, shipboard XRF samples, squeeze-cake residues from interstitial-water studies, "bomb," and "REV" (Rock-Eval) samples collected during shipboard sampling. The weight percent (wt%) of carbonate carbon was determined by reacting approximately 20 mg (accurately weighed) of ground sample in a 2N HCl solution. The quantity of CO₂ liberated was measured by titration in a monoethanolamine solution with a colorimetric indicator. The change of transmittance was monitored by a photo detection cell. Total carbon values were measured by combustion of bulk samples at 960°C in an oxygen atmosphere, converting both organic and inorganic forms of carbon to CO₂, which was then quantitatively analyzed by the coulometric titration method outlined above. Total organic carbon contents were then determined by subtracting the values for carbonate carbon from the total carbon content. Carbonate carbon and total carbon values reproduced well, and standard deviations for replicate analyses usually did not exceed 1%. Organic carbon concentrations were also determined by Rock-Eval as an alternative method.

Rock-Eval Method

The bulk geochemical character of sedimentary organic matter was determined using the Rock-Eval pyrolysis techniques outlined by Espitalié et al. (1977). The following parameters were measured during the programmed pyrolysis (300° to 600°C) of 100-mg ground bulk samples: the amount of "free" hydrocarbons released at 300°C (S_1), the amount of hydrocarbons released during heating to 600°C (S_2), which is mainly caused by cracking of kerogen, total CO₂ released from organic matter during pyrolysis to 390°C (S_3), the temperature of maximum hydrocarbon release during pyrolysis (T_{max}), and the total amount of CO₂ generated during oxidation at 600°C. Hydrogen, oxygen, and productivity indexes and total organic carbon concentrations were calculated from these values. The hydrogen index represents the ratio of pyrolyzable organic matter or "hydrocarbons" (S_2) to total organic carbon (mg HC/g TOC). The oxygen index represents the ratio of CO₂ released (S_3) to total organic carbon (mg CO₂/g TOC). The production index (PI) is defined as the ratio $S_1/S_1 + S_2$.

Hydrocarbon Gases

For safety considerations, the concentrations of C₁ (methane) and C₂ (ethane) hydrocarbon gases were monitored in cores at 10-m intervals. Gases were extracted from bulk sediments using a headspace-sampling technique (Emeis and Kvenvolden, 1986). Headspace analyses were performed on about 5 cm³ of core that was placed in a glass container sealed with a septum and metal crimp and then heated to 70°C. All headspace gas samples were analyzed with a Carle AGC 1000/Model 211. Gases were also measured in sediments with a Hewlett Packard 5890 Natural Gas Analyzer (NGA). This chromatograph is fitted with Porapak T, Molecular Sieve, and capillary columns and both thermal conductivity (TCD) and flame ionization (FID) detectors. The details of the configuration of the NGA gas chromatograph are available in Kvenvolden and McDonald (1986). Gases measured with the NGA include, oxygen, nitrogen, carbon dioxide, carbon monoxide, hydrogen sulfide, and the suite of C₁ to C₆ hydrocarbons. Approximately 7 cm³ of wet sediment was sealed in a glass container and then immediately flushed with helium at a flow of about 150 cm³/min for two minutes. The vial was heated at 70°C for about 45 min and a 5-cm³ sample of headspace injected into the NGA. The headspace and wet sediment volumes were measured at the completion of the gas chromatograph analysis.

SEDIMENT INORGANIC GEOCHEMISTRY

Interstitial Water

Shipboard interstitial-water analyses during Leg 123 were performed on sections of whole-round sediment cores 3 to 10 cm long. Samples were collected as soon as the core arrived on deck and were taken from every core (about 10 m apart) to a depth of 100 mbsf and from every third core (about 30 m apart) below 100 mbsf, when sufficient material was available. Samples were initially cleaned by scraping off the exterior surface with a stainless steel spatula and then squeezed in a stainless steel press for time periods of up to 2 hr (usually 10 to 20 min) to 30,000 to 40,000 psi at room temperature (Manheim and Saylor, 1974). After filtration through a 0.45- μ m filter, the interstitial-water samples were analyzed for pH, alkalinity, salinity, chloride, sulfate, calcium, magnesium, silica, ammonium, phosphate, and manganese; alkalinity, pH, and salinity were determined immediately after filtration, and samples were then refrigerated and titrations and instrumental analyses performed within a few days after sample collection. All shipboard chemical analyses of interstitial waters followed standard ODP techniques. The potentiometric titration of alkalinity and measurement of pH were conducted using a Metrohm autotitrator and a Brinkman combination pH electrode (Gieskes, 1974). The amount of total dissolved solids (salinity) was determined using a Goldberg optical refractometer. Calcium, magnesium, and chloride concentrations were determined titrimetrically, as described by Gieskes (1974) and modified by Gieskes and Peretsman (1986). Sulfate was determined using a Dionex ion chromatograph (Gieskes and Peretsman, 1986). Colorimetric methods employing a Bausch and Lomb Spectronic 1001 spectrophotometer were used to determine the concentration of silica (Gieskes and Peretsman, 1986), ammonium (Solorzano, 1969), phosphate (Strickland and Parsons, 1968; Presley, 1971), and manganese (Brewer and Spencer, 1971). International Association of Physical Sciences Organizations (IAPSO) standard seawater was used to standardize all analyses. Potassium and strontium were analyzed post-cruise in an onshore laboratory by atomic absorption spectrometry.

Mineralogy

Mineralogy of the pressed whole cores (squeeze cakes) was determined by X-ray diffraction. After extraction of the interstitial water, bulk squeeze-cake samples were oven-dried at 60°C overnight, weighed, and washed through a 38- μ m sieve with deionized water. Most samples were placed in an ultrasonic bath for several minutes to help disaggregate and suspend the clay-sized particles. The 2- through 38- and <2- μ m size fractions were separated by centrifuge (3000 rpm for 1 min and 3000 rpm for 18 min, respectively), and the <<2- μ m suspension was separated by a 0.6- μ m filter. Sodium pyrophosphate (5 wt% solution) was added to some samples to prevent clay flocculation. The bulk and separated size fractions were run as standard powder mounts on a Philips APD 3720 automated XRD system. The <<2- μ m size fraction was run as an oriented slide (air-dried filter attached directly to XRD sample holder using petroleum jelly) and rerun after ethylene glycol treatment. The Philips XRD is equipped with a monochromator and scintillation detector, and uses CuK α X-radiation. The XRD generator was set at 40 kV and 35 mA (see "XRD Analyses" section, this chapter, for more discussion of the XRD procedures).

PHYSICAL PROPERTIES

The physical properties determined on board ship were compressional-wave velocity, porosity, bulk density, grain density, water content, thermal conductivity, and undrained shear strength.

The Gamma-Ray Attenuation Porosity Evaluator (GRAPE), described by Boyce (1976), was used to measure continuously the wet-bulk density in HPC cores only, as the tool required close contact between the sediments and the core liner. Aluminum and water standards were used for calibration before each site. The core section to be measured was mounted vertically in a rack, and the gamma-ray source and sensor moved down the length of the core. The attenuation of the gamma rays passing through the liner and core was measured every 1.5 to 2.0 cm, and the density was calculated from the attenuation values.

The *P*-wave Logger (PWL) was mounted on the same frame, and hence performed simultaneously with the GRAPE. Two 500-kHz compressional-wave transducers were aligned perpendicular to the core axis and moved down the length of the core. Measurements were taken at 2 cm intervals. Water was applied to the core liner to improve acoustic contact.

After GRAPE and PWL measurements, the cores were allowed to equilibrate to room temperature for 3+ hr before thermal conductivity was measured. The thermal conductivity techniques used here have been described by Von Herzen and Maxwell (1959) and Vacquier (1985). Needle probes connected to a Thermcon-85 unit, interfaced with a PRO-350 computer, were inserted into the sediment through holes drilled into the liner, and thermal drift was monitored. An additional probe was inserted into a reference material. Once the temperature had stabilized, the probes were heated, and the coefficient of thermal conductivity was calculated as a function of the change in resistance in the probe about every 12 s over a 6-min interval.

When the sediment became too stiff to allow us to insert the probe, holes were drilled with a long, thin drill bit. Thermal conductivity measurements on well-lithified sediments were conducted on split cores with the use of a needle probe partially embedded in a slab of insulating material. The sample was placed on the slab, immersed in a saltwater bath, and allowed to reach thermal equilibrium with the water. The probe was heated, and resistance changes in the probe were measured every 9 s for a 6-min interval. Good contact with both slab and sample was accomplished using Dow Corning 111 heavy silicone lubricant between the slab and sample.

Undrained shear strength of the sediment (described by Boyce [1977] and Lee [1984]) was determined using a Wykeham Farrance motorized vane apparatus with a four-bladed vane having a diameter of 1.28 cm and a length of 1.28 cm. This vane was inserted into the split core section perpendicular to its face i.e., perpendicular to the core axis, to a point where the top of the blade was covered by sediment. The vane was then rotated at a rate of about 90°/min until the sediment failed. The undrained shear strength was calculated from the peak torque obtained at failure.

Electrical resistivity of the sediments was not determined on any cores during Leg 123 because of equipment malfunction.

Compressional-wave velocity measurements, in addition to those described above, were taken on samples adjacent to intervals for which undrained shear strengths were determined. Velocities were calculated from the determination of the traveltime of a 500-kHz compressional wave through a measured thickness of sediment sample using a Hamilton Frame Velocimeter and Tektronix DC 5010 counter/timer system. Travel distance was measured by using an attached variable resistor connected to a Tektronix DM 5010 digital multimeter. Samples were taken by either cutting parallel-sided pieces with a knife in the softer sediments, or using a double-bladed diamond saw for the more brittle or lithified sediments. Basement rock samples were obtained using a 2.5-cm rock corer.

The Hamilton Frame was calibrated with lucite, aluminum, brass, and water standards at the beginning of Leg 123, and we found that a correction factor of 1.0347 was needed to bring all

measured values into agreement with calibration values. The variable resistor was calibrated with standard lengths of aluminum cylinders.

The index properties of wet-bulk density, grain density, porosity, and water content were determined on the same samples as those used to measure velocity. This enabled us to apply direct cross correlation to the data to check for trends and data consistency. Samples were weighed wet using two Scientech 202 electronic balances, interfaced with a PRO-350 computer, which compensates for the ship's motion by taking the average of 100 sample weighings. The wet sample volumes were then determined by using a Quantachrome helium Penta-Pycnometer. Dry sample weight and volume were determined using the same procedure after freeze drying the sample for 12 hr. However, we found that dry sample volumes determined with the Penta-Pycnometer were often higher than the wet volumes for basalt cores. For these samples, the sample total value was determined from the dimensions of the cylindrical plug measured with a Vernier caliper. (It was subsequently found that a systematic error existed in the measured values of wet volume.)

The definitions used for the index properties are:

1. Porosity (%) = $100 \times \text{volume of water/volume of wet sediment}$.
2. Bulk density (g/cm^3) = $\text{weight of wet sediment/volume of wet sediment}$.
3. Grain density (g/cm^3) = $\text{weight of dry sediment/volume of dry sediment}$.
4. Water content (%) = $100 \times \text{weight of water/dry weight of sediment}$.

Dry-sediment weights and volumes used in the above calculations were corrected for salt content (assuming seawater salinity of 35‰) by subtracting the estimated weight and volume of residual salt.

The data were entered into the shipboard Physical Properties Data Collection System. This system computes the depth below seafloor, index properties, shear strength, and velocities for each sample.

The physical properties collected for samples during Leg 123 are presented in tables and figures in each site chapter. Porosity (ϕ), bulk density (ρ), and velocity (V) values are given in the "Physical Properties" column on the barrel sheets for the cores of each site.

XRD ANALYSES

A Philips ADP 3520 X-ray diffractometer was used for XRD analysis of unknown secondary mineral phases. Instrument conditions were as follows:

CuK α radiation with nickel filter
 40 kV
 35 mA
 Goniometer scan from 2° to 70° 2 θ
 Step size 0.02°
 Count time 1 to 2 s

XRD analyses were completed on bulk samples and on samples from Holes 765B and 765C using the fraction finer than 2 μm . For powder diffraction analyses, samples were ground using the Spex 8000 Mixer Mill or, when there was little sample material, using an agate mortar and pestle. The material was then pressed into aluminum sample holders for X-ray analysis.

For clay mineralogy, both powder residues and bulk samples were used. The preparation method is similar for both types of samples, except for the sieving step. Samples were treated with distilled water to disaggregate the components and then sepa-

rated into the fractions $>38 \mu\text{m}$, 2 through $38 \mu\text{m}$, and $<2 \mu\text{m}$. This separation was obtained by sieving with a $38\text{-}\mu\text{m}$ -mesh sieve, followed by a 3-min centrifuging step. The suspension was decanted and again centrifuged for 15 min. The resulting suspension was assumed to contain the fraction less than $2 \mu\text{m}$. This suspension was washed through a $0.6\text{-}\mu\text{m}$ filter. The method led to a good orientation of the clay minerals. A piece of the filter was mounted on an XRD sample holder using petroleum jelly. Finally, the samples were analyzed on both nonglycolated and glycolated bases.

XRD analyses give only qualitative estimates of mineral composition. Therefore, the results were plotted using the relative peak intensity of each mineral as follows: for bulk samples the strongest peak (the dominant mineral) was assigned a value of 40%, followed by up to two major components, each with 20%; minor components (up to four) were assigned values of 5%; samples containing only one mineral (e.g., washing residues) were plotted as 100% for this mineral. For the clay minerals a similar method was used, with the difference that the total composition always equaled 10. Resulting diffractograms were interpreted with the help of a computerized search-and-match routine using the Joint Committee on Powder Diffraction Standards (JCPDS) powder files and tabulated data for clay minerals in Chen (1977). See "Sediment Inorganic Geochemistry" section, this chapter, for further discussion of XRD methods.

XRF ANALYSES

During Leg 123, the fully automated ARL 8420 wavelength-dispersive X-ray fluorescence (XRF) system available on board *JOIDES Resolution* was used to determine the major oxide compositions and trace-element abundances of whole-rock and sediment samples.

Analyses of the major oxides were performed on lithium borate glass disks doped with lanthanum (La) as a "heavy absorber." This technique is similar to that developed by Norrish and Hutton (1969). Samples were dried and crushed in a tungsten carbide shatterbox. Powders made from igneous rock samples were ignited for 2 hr at about 1030°C , while sediment samples were ignited for 2 hr at 450°C , followed by 3 hr at 1000°C . A total of 500 mg of the ignited powder was mixed with 6.0 g of dry flux consisting of 80% lithium tetraborate and 20% La_2O_3 . This mixture was then melted at 1150°C in a platinum-gold crucible for a maximum of 10 min, then poured into a platinum-gold mold using a Caisse Fluxer. The 12:1 flux to sample ratio chosen was sufficient to eliminate matrix effects over a certain range of rock compositions in such a manner that X-ray intensity and concentration simply relate linearly:

$$c_i = (I_i \times m_i) - b_i,$$

where

- c_i = concentration of oxide (wt%),
- I_i = net peak X-ray intensity of oxide i ,
- m_i = slope of calibration curve for oxide i (wt%/cps),
- b_i = apparent background concentration for oxide i (wt%).

The slope m_i was calculated from a calibration curve derived by measuring a set of well-analyzed "standards" (reference rocks). The background b_i was either determined on blanks or derived mathematically from the calibration curves. Analyses were performed on both sedimentary and igneous rocks cored during Leg 123. To cover the range of compositions encountered, SPEX SiO_2 and CaCO_3 were used when constructing the calibration curves; both standards were used for the sediments where Si-poor calcareous oozes and Ca-poor siliceous oozes were analyzed. The Ca-rich standard was not used for calibrating igne-

ous rocks. With the exception of moving the background for magnesium (Mg) to avoid interference for the Ca $K\alpha$ III-order line in Ca-rich samples, the machine operating conditions for the major elements were identical to those employed during Leg 111, when the XRF system was first calibrated (Becker, Sakai, et al., 1988). A synthetic, high-concentration standard was used to monitor machine drift, and a standard was run with every batch of six unknowns.

For the major elements, all samples were ignited. The chemical composition of these rocks thus was determined on a water-free and CO_2 -free basis, with all iron (Fe) having been oxidized to Fe_2O_3 . Variation of the major oxide sums of ± 0.5 wt%, for the igneous rocks, were considered reasonable. For the sediments, given the high organic carbon (C), sulphur (S), and trace-element contents of some samples, totals as low as 98.0 wt% were accepted. A significant problem was the loss of potassium (K) and sodium (Na) during ignition of the sediments. To correct for this problem, K, Na, phosphorus (P), and manganese (Mn) were analyzed using the same pressed powders that were used for the trace-element analyses. Calibration curves were constructed by linear regression. Mass-absorption corrections were calculated for siliceous and carbonate matrices, but these corrections were insignificant considering the precision of the analyses (5%–10%). Uncorrected data were used, and the major elements determined in the fused glasses were corrected by factors corresponding to the extent of loss of volatiles. Results for repeated analyses of the sediment standard SCO-1 (Cody Shale) are presented in the "Sediment Inorganic Geochemistry" section of the Site 765 chapter.

Trace-element determinations for both the igneous rocks and the sediments were performed on pressed-powder pellets prepared by pressing (with 7 tons of pressure) a mixture of 5.000 g of dry rock powder (dried at 110°C for >2 hr) and 30 drops of polyvinyl-alcohol binder into an aluminum cap. A subset of sediment samples was ignited and then pressed into powder pellets to evaluate volatile-free determinations relative to analyses recalculated on a carbonate-free basis; with the exception of rubidium (Rb), which underwent extensive loss in the carbonate-rich samples, the trace element "enrichments" in the ignited samples were consistent with the determined loss on ignition. To evaluate contamination from seawater, a second subset of powders was washed and centrifuged before preparing the pressed-powder pellets. Analyses of these rocks, within error limits, were comparable to the unwashed samples for the trace elements studied, but there was a substantial loss of Na_2O in some samples during washing.

A modified Compton scattering technique based on the intensity of the rhodium Compton peak was used for matrix absorption corrections (Reynolds, 1967). A comprehensive description of this analytical procedure is given in the "Introduction and Explanatory Notes" chapter in the *Initial Reports* volume of Leg 111 (Becker, Sakai, et al., 1988). The elements niobium (Nb), zirconium (Zr), yttrium (Y), Sr, Rb, copper (Cu), zinc (Zn), nickel (Ni), chromium (Cr), vanadium (V), titanium (Ti), and barium (Ba) were determined in the igneous and sedimentary rocks. Overlap corrections were made for: Y $K\beta$ on Nb $K\alpha$; Sr $K\beta$ on Zr $K\alpha$; Rb $K\beta$ on Y $K\alpha$; V $K\beta$ on Cr $K\alpha$; Ti $K\beta$ on V $K\alpha$; cesium (Ce) $L\beta$ on Ba $L\alpha$. All of the carbonate-rich sediments contained Sr abundances in excess of 2000 ppm. While the calibration for Sr remained linear at these concentrations, the overlap correction for Zr $K\alpha$ was not linear; the estimated correction of 8.5% of the Sr $K\alpha$ peak at the Zr $K\alpha$ position was at least an order of magnitude too large. Rather than assume a nonlinear calibration, Zr analyses for the sediments were performed using the Zr $K\beta$ peak. This proved very satisfactory and, even for samples with Sr values of <500 ppm and despite the lower intensities of the $K\beta$ peak, errors in Zr $K\beta$ determinations

remained comparable to those of the Sr-corrected Zr $K\alpha$ peak. The calculated concentrations of trace elements for SCO-1 and standard deviations, and means for replicate analyses, are given in the "Sediment Inorganic Geochemistry" section of the Site 765 chapter.

Table 3 presents a compilation of all XRF analyses of the Mid-Atlantic Ridge basalt standard AII-92-29-1 (Staudigel, 1980) from Leg 111 to the end of Leg 123. To correct for slight calibration inconsistencies, the entire XRF data set was normalized to the recommended values for AII-92-29-1 given in Table 3.

BASEMENT STRESS MEASUREMENTS

Anelastic Strain Recovery Experiments

The Ocean Drilling Program provides an excellent opportunity to determine the state of stress in ocean crust in different tectonic regions. Anelastic strain recovery experiments, conducted at Sites 765 and 766 during Leg 123, have never before been applied to oceanic rocks. These experiments form part of a more comprehensive shore-based study to develop an integrated understanding of the relationship between rock fabric anisotropy, static and dynamic rock characteristics, and the magnitudes and directions of the principal horizontal stresses.

Stresses in the oceanic crust arise from plate-driving forces, from temperature changes, from gravitational loading by volcanics and sediments, and from poorly understood mid-plate tectonics. The magnitude and direction of the principal stresses in the brittle crust influence the propagation of faults, the opening and closing of cracks, and pore-water circulation. A knowledge of the state of stress provides insight into past tectonic history and likely future tectonic development of a region and also into the mechanism of plate motions.

The recently developed technique of anelastic strain recovery is potentially able to determine directions and magnitudes of the principal stresses by measuring the changes in geometry of the recovered core with time (Teufel and Warpinski, 1984). However, a study of stress should include how the results of experi-

mental measurement can be influenced by intrinsic elastic properties and rock characteristics and also how interpretation may be improved by a knowledge of these properties. An integrated approach was adopted by a consortium of the British Geological Survey, the Imperial College of Science and Technology, the University of East Anglia, and the Institute of Oceanographic Sciences, all in the United Kingdom. This integrated approach includes studies of anelastic strain recovery, differential strain analysis, dynamic and static rock properties at *in-situ* pressures and temperatures, scanning electron microscopy, and fundamental theory.

To maintain confidence in the integrity of the theoretical relationships between the measured parameters, the measurement scale must be compatible. These compatible sets of core-scale measurements can be used, together with the downhole logging, hydraulic fracturing, and televiwer (borehole-scale) measurements, to construct a more comprehensive understanding of the relations between rock stress, rock structure, pore pressure, and crustal tectonics. That is, we must be sure we can extrapolate core- and borehole-scale measurements to the wider field.

Theoretical Aspects

Stress is a quantity that cannot be measured directly, but only derived by way of a relationship with strain or some other indicator. The major group of stress indicators rely on correlation with strain relief mechanisms and associated rock deformation. The release of *in-situ* stress can generate microcracks through the differential expansion of adjacent grains (Nur and Simmons, 1970). Evidence of cracks generated in this manner for rock samples recovered from deep boreholes has been summarized by Kowallis and Wong (1983). The strain associated with relaxation of *in-situ* stored strain energy generally involves both an instantaneous elastic component and a time-dependent (anelastic) component. Voight (1986) first suggested that if one assumes that a proportion of the time-dependent strain is proportional to the total recoverable strain, then one can estimate the *in-situ* stress state at depth by measuring rock cores immediately upon removal from the borehole. Anelastic strain-relaxation techniques measure this time-dependent component of strain, whereas differential strain analysis correlates crack densities, formed in part instantaneously and in part time dependently, with *in-situ* stress.

At present, the theoretical analysis of anelastic strain recovery measurements (Blanton, 1983; Warpinski and Teufel, 1986) does not adequately account for the effect of pore-pressure dissipation during strain relief. Numerical modeling and closed-form solutions will be used to improve the interpretation of results obtained during Leg 123, especially the phenomenon of observed core contraction (Teufel, 1986).

Shipboard Measurements

When a core is drilled out of *in-situ* rock, the anelastic strain component is recovered over a period of between 20 to 50 hr, depending upon the elastic characteristics of the rock and the relative magnitudes of the maximum and minimum principal horizontal stresses (S_H and S_h). Teufel and Warpinski (1984) devised a rig that, when placed over a segment of core, can monitor the physical changes during this period. British Petroleum Research (Sunbury) United Kingdom, modified these measuring techniques, which have been further improved by the British Geological Survey (BGS) during the equipment construction phase of this project.

The essentials of the BGS equipment are as follows:

1. A set of five strain transducers, four of which are held by carbon fiber rings at pre-determined relative positions around a 20-cm whole-round rock sample and one along the long axis of

Table 3. Major and trace element data for the standard AII-92-29-1A analyzed on ODP Legs 111 to 123.

	Leg 111	Leg 133	Leg 115	Leg 121	Leg 123	Recommended
Major elements						
SiO ₂				49.74	49.51	49.80
TiO ₂				1.74	1.85	1.73
Al ₂ O ₃				15.78	15.53	15.41
Fe ₂ O ₃				10.67	10.83	10.97
MnO				0.19	0.18	0.18
MgO				7.49	7.50	7.58
CaO				11.06	11.09	11.07
Na ₂ O				2.96	3.1	3.00
K ₂ O				0.17	0.17	0.16
P ₂ O ₅				0.16	0.15	0.18
No.				18	18	
Minor elements						
Nb	3.5	3.4	4.3	2.6	3.1	3.1
Zr	128	128	130	126	129	130
Y	39	40	41	39	40	39.4
Sr	129	129	129	132	126	133
Rb	1.3	1.3	1.3	1.4	1.0	1.0
Zn	89	87	85	93	86	81
Cu	66	63	63	59	62	62
Ni	101	106	103	114	105	103
Cr	249	240	238	227	239	292
V	299	301	292	297	302	304
Ce		10	8		17	13
Ba		6	18		6.7	5.9
No.	9	8	9	18	13	

the sample. In addition, a sixth strain transducer sets across a glass ceramic disk of zero coefficient of thermal expansion so that any extraneous effects of temperature on the equipment can later be removed from the experimental results.

2. The rock sample, together with the strain transducers and a temperature measuring sensor, is placed on a frame inside a thermally insulated container that is filled with an inert Dow Corning silicon fluid. The silicon fluid and the thermally insulated container serve to minimize the effects of laboratory temperature fluctuations and also to eliminate any stress-related effects from drying out of the rock. In addition, a fluid having sufficient viscosity was chosen to dampen out potential vibrations transmitted from the ship to the sensitive strain transducers. The limit of measurement sensitivity is less than $0.1 \mu\text{m}$.

3. A portable microcomputer, interfaced to the strain transducer and temperature sensor electronic control unit, which acts as a data logger to record directly into a Lotus spreadsheet.

Up to three rock cores may be monitored at a time, and the equipment is set to collect and record data at intervals of between 1 and 3 min for a period of up to several days without attendance. Built-in software provides for preliminary interpretation and plotting of data, but a complete interpretation depends upon additional information retrieved from each individual rock sample on shore.

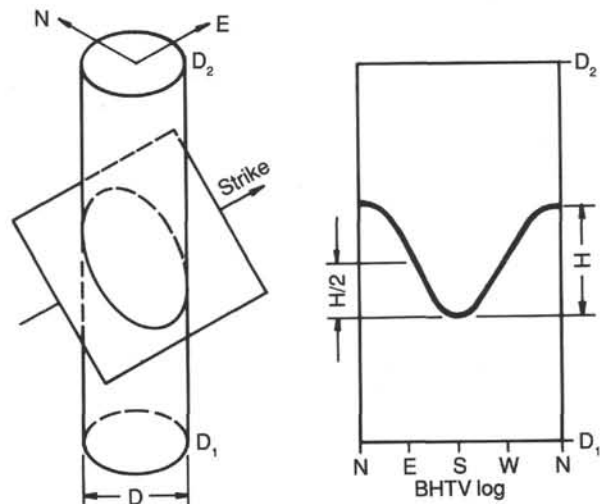
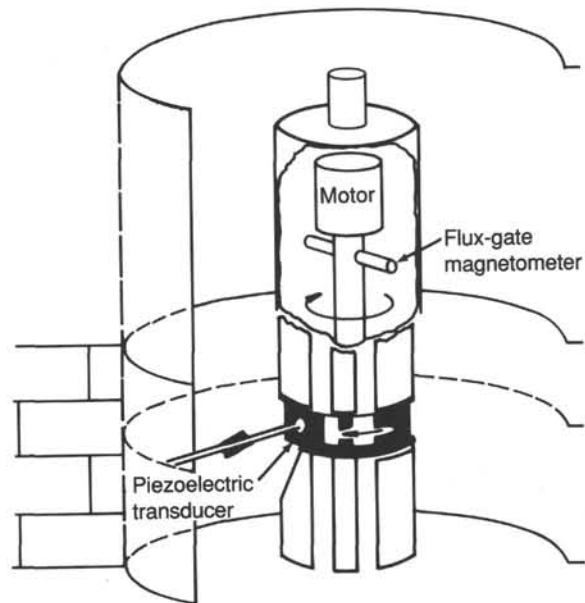
In-Situ Stress Measurements

In-situ stress measurements have been conducted in continental drill holes for more than 30 yr. These measurements have yielded a wealth of information covering a wide range of scientific disciplines ranging from civil engineering, earthquake research, fault mechanics, to research directed toward understanding the driving forces associated with plate tectonics.

Stanford University is under a subcontract with Lamont-Doherty Borehole Research Group for the adaption of specialty logging services that include the borehole televiewer, multichannel sonic tool, and hydraulic fracturing experiments.

Borehole Televiewer (BHTV)

The borehole televiewer is an ultrasonic, high-resolution logging tool used to measure the geometry of the borehole wall, fracture, and lithostratigraphic features. The BHTV, originally designed by Mobil Oil Inc., contains a rotating acoustic transducer that emits a focused 3° beam pulse at a rate of 1800 times/s (Fig. 13). The BHTV can operate in low-frequency mode, using the 400-kHz transducer, or in high-frequency mode, using the 1.4-MHz transducer. The high-frequency transducer is designed to resolve detailed features, such as fracture density and fracture aperture (the amount of fracture opening). Although the low-frequency transducer can detect fractures, it is best suited for delineating the geometric texture of the borehole wall, such as spalling or wellbore breakouts. Orientations of all these features are acquired by using a fluxgate magnetometer that triggers the signal at each crossing of magnetic north, while the tool is pulled uphole at a rate of 2.5 cm/s. A reflectance image of the borehole wall is obtained in real time by windowing the acoustic reflection off the borehole wall and recording this on Polaroid film. The raw output consists of full-waveform acoustic seismograms that are also recorded on videotape for later reprocessing. The traveltimes and the degree of acoustic reflectance from these data can then be used to determine a more accurate three-dimensional image of the borehole geometry, as well as to delineate the textural characteristics of the borehole wall. The BHTV is a valuable tool for analyzing borehole breakouts. Stress-induced wellbore breakouts are elongated zones of spalling along cylindrical holes in rocks (Fig. 14). These breakouts commonly span a few tens of degrees of circumference. In an



Strike: Orientation of midpoint between peak and trough
(at $H/2$)

Dip: $\tan^{-1} H/D$

Figure 13. A schematic showing the BHTV with the piezoelectric transducer, which emits acoustic pulses at a rate of 1800/s. The magnetometer is used to record the orientation of the reflected images. The cartoon on the right shows how a dipping feature in the borehole appears on a BHTV record. The image of the borehole is opened up, and the orientation can then be determined.

isotropic, linearly elastic rock subject to differential stresses, breakouts form along the borehole wall as a result of compressive stress concentrations exceeding the strength of the rock. Under these conditions, the breakout orientation will develop in the direction of the least principal horizontal stress. It has been demonstrated in different areas that stress orientations deduced from breakouts are consistent with other independent indicators (Bell and Gough, 1979; Zoback and Zoback, 1980; Shamir et al., 1988; Zoback et al., 1988).

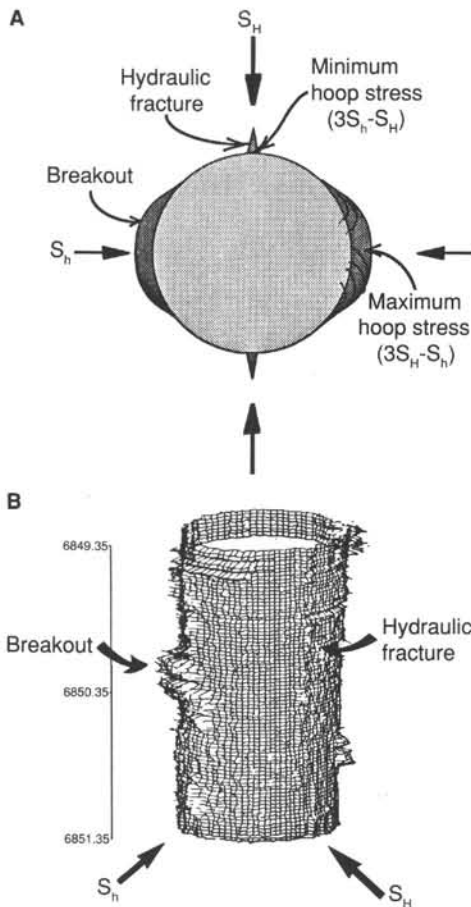


Figure 14. A. Illustration showing the distribution of stress concentrations in a circular hole in an elastic medium. Given the orientations of the principal stresses, S_H and S_h , the direction along which the hydraulic fracture will parallel the S_H direction, while the breakouts will preferentially be oriented parallel to the S_h direction. The points of minimum and maximum stress concentration are called the hoop stresses. B. An oblique view of the borehole wall derived from BHTV images. The direction of the principal stresses can be inferred from the orthogonality of the stress induced breakouts and the trend of the hydraulic fracture.

Hydraulic Fracturing Experiment (Hydrofrac)

In-situ stress magnitudes at great depths (> 1 km) are commonly measured using the hydraulic fracturing technique (hydrofrac). When conducting a hydrofrac test, a 1.5-m-long section of the borehole is isolated with inflatable steel-reinforced rubber packers. Once the packers have been inflated and pressed up against the borehole wall, pressure is then applied to the test interval until the borehole pressure exceeds the tensile stress concentration along the borehole walls (Figs. 14 and 15). At the failure point, the pressure decreases markedly as the hydraulic fracture propagates away from the borehole wall. Repeated pressurization cycles are conducted to propagate the vertical fracture several meters away from the hole. The purpose is to isolate the far-field stresses operating on the hydraulic fracture from any perturbations in the ambient stress field induced by the hole itself.

Theoretical Aspects

In the hydraulic fracturing technique, one of the principal stresses (S_v) is assumed to be parallel to the borehole; the other two principal stress directions are assumed to be parallel to the Earth's surface and mutually orthogonal. It is further assumed

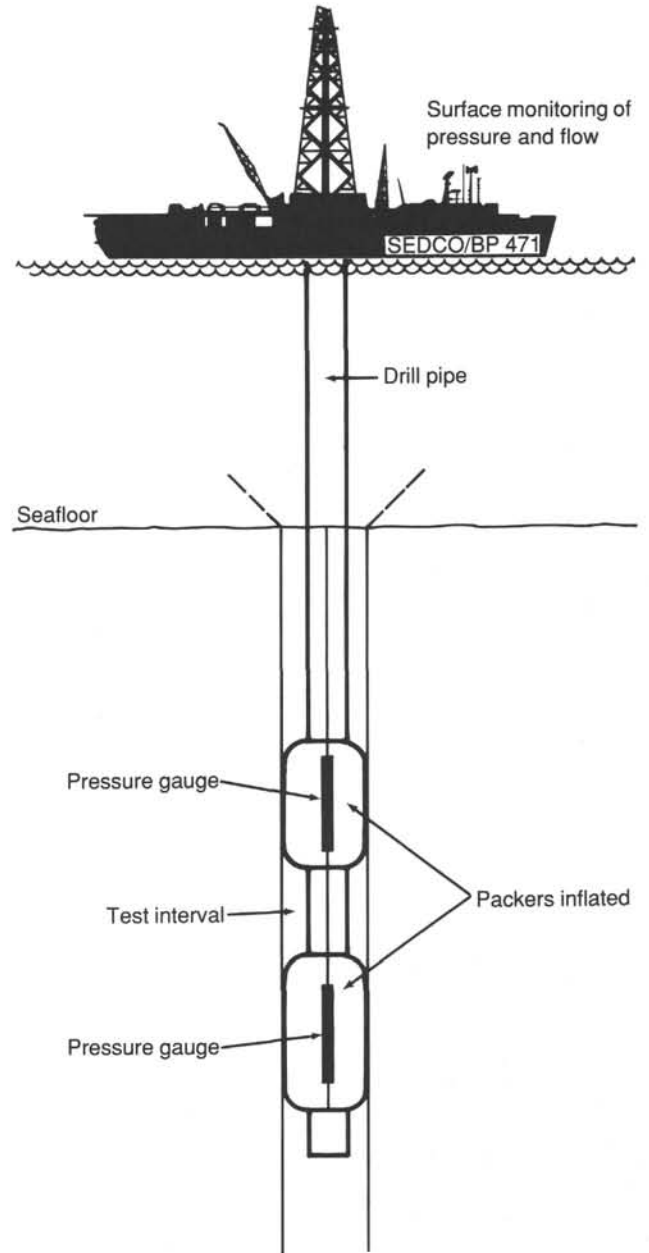


Figure 15. A schematic of hydrofrac operations showing the inflatable packers in their inflated configuration. The isolated test interval, between the packers, is pressurized by pumping fluids through drill pipe and monitoring the pressure both downhole and at the surface. Multiple cycles of applying pressure and then releasing pressure within the test interval are done to propagate the hydraulic fracture away from the borehole and thus record accurate estimates in a stress field far removed from the borehole. At the end of a test, the packers are deflated and moved to the next location.

that the hydrofrac propagates in the direction perpendicular to the minimum horizontal principal stress (S_h) or parallel to the maximum horizontal principal stress (S_H) direction. The assumption that the hydrofrac propagates perpendicular to S_h is supported by experimental and theoretical investigations (Haimson and Fairhurst, 1970). The magnitude of pressure in the fracture immediately after pumping, when the well is shut in. This pressure is interpreted as being the pressure necessary to keep the fracture open and therefore balanced against S_h . Determination of S_H requires the assumption of the elastic concentration of

stresses around the circular borehole wall. Where wellbore breakouts occur, the elastic stress concentrations are sufficiently distorted to warrant avoiding using these zones in a hydrofrac experiment. For this reason, BHTV data are collected before performing hydrofrac experiments to locate those intervals best suited for stress measurements.

Hydrofrac Procedure

The basic procedure for conducting hydrofrac tests is as follows: (1) to inflate the rubber packers and straddle the test interval; (2) to conduct multiple cycles of applying and releasing pressure within the test interval, increasing pumping times for each subsequent cycle; (3) to pump at the same flow rate for each cycle; (4) to permit flowback on each cycle, allowing for drainage of excess fluid pressure from the fracture; (5) to deflate packers and move packer arrangement to next test location. After the packers are brought back to the surface, a BHTV log is run to determine the orientation of the hydraulic fracture as well as to document any changes in the stress-induced breakouts with time (Fig. 14).

Interpretation of Pressure Records

The theoretical foundation for interpreting hydrofrac pressure data, as was initially suggested by Hubbert and Willis (1957) and later formulated by Haimson and Fairhurst (1970), is the classic breakdown equation,

$$P_b = 3S_h - S_H - P_p + T,$$

relating the breakdown pressure, or the presumed pressure necessary to generate a hydrofrac, P_b , to the horizontal principal stresses, S_H and S_h , the formation pressure, P_p , and the tensile strength of the intact rock formation, T . The pore-pressure term is the hydrostatic pore pressure that can be calculated for any depth below sea level. The magnitude of S_h is equivalent to the shut-in pressure observed from the pressure-time records. Bredehoeft and Papadopoulos (1980) were the first to suggest that S_H could be determined without knowledge of T by using the pressure needed to reopen a preexisting hydraulic fracture, $P_b(T = 0)$. Placing $T = 0$ in the above equation, we have

$$P_b(T = 0) = 3S_h - S_H - P_p,$$

or

$$S_H = 3S_h - P_p - P_b(T = 0),$$

which is an expression for the maximum horizontal stress in terms of the shut-in, pore, and fracture-reopening pressures.

GEOPHYSICAL WELL LOGGING

Geophysical well logging provides continuous, *in-situ* measurements of physical and chemical formation parameters, which upon interpretation yield stratigraphic, lithologic, geophysical, and mineralogic characterizations of the site. Logging data may be correlated directly with core measurements when available, or may be used to supplement the data set when core recovery is poor. The Lamont-Doherty Borehole Research Group has been contracted by ODP to provide the geophysical well logging on board the *JOIDES Resolution*. Lamont-Doherty, in turn, sub-contracts Schlumberger Offshore Services to run the downhole logging tools. While the logging tools used by Schlumberger are designed for use in petroleum exploration, many have proved useful for gathering information of scientific interest. In some cases, individual logging sondes have been modified to meet ODP requirements, including the reduction of tool diameter to allow for insertion in the 3.8-in. drill string bore.

The various Schlumberger logging tools are combined into three tool strings for maximum efficiency. These tool combinations are the seismic stratigraphic, the litho-porosity, and the geochemical combinations. The seismic stratigraphic combination string includes (1) the long-spaced sonic tool (LSS); (2) dual-induction (DIL) or phasor-induction tool (DITE); (3) a gamma-ray (GR) or natural gamma-ray spectrometry tool (NGT); and (4) a caliper tool (MCD). This tool combination measures compressional-wave velocity, resistivity, and hole size, and estimates the proportions of the primary radioactive elements uranium (U), K, and thorium (Th).

The litho-porosity combination string includes (1) natural gamma-ray spectrometry measurements (NGT); (2) a litho-density tool (LDT); and (3) a compensated-neutron tool (CNT-G). This combination provides measurements of formation porosity and density, and determines the spectral content of naturally occurring radiation.

The geochemical combination string includes (1) natural gamma-ray spectrometry (NGT); (2) induced gamma-ray spectrometry measurements (GST); and (3) the aluminium clay tool (ACT). This tool combination measures the relative concentrations of 11 elements: Si, Ca, Al, Fe, S, Mn, hydrogen (H), chlorine (Cl), K, Th, and U. Two additional tools (the three-axis magnetometer [GPIT] and auxiliary measurement sonde [AMS]) can be run on either the litho-porosity or geochemical tool strings. The GPIT measures vector magnetic field, hole azimuth, and hole deviation. The AMS measures hole temperature and mud resistivity.

A brief outline of the operation of each tool used during Leg 123 follows. Further information may be obtained from the Borehole Research Group at Lamont-Doherty Geological Observatory, the ODP Wireline Logging Manual, or directly from Schlumberger.

Long-Spaced Sonic and Array Sonic Tools

The LSS and SDT tools measure the compressional-wave velocity of the formation. A series of 50-Hz acoustic sources at a fixed spacing and a corresponding set of receivers are configured to provide interval traveltime in microseconds per foot for the receiver pairs at various distance configurations. Common source-receiver distances are 8, 10, and 12 ft. This arrangement compensates to some extent for borehole fluid velocity and hole rugosity. These data are processed to yield formation velocity, which, when combined with the formation density, can be used to generate a synthetic seismogram.

Dual-Induction (Model E)/Phasor-Induction Tool

The DITE tool provides three measurements of formation resistivity:

1. Deep induction (Induction Log-Deep: ILD);
2. Medium induction (Induction Log-Medium: ILM);
3. Shallow induction (Spherically Focused Log: SFL).

Each measurement has a characteristic depth of investigation that depends on the formation, pore fluid, and mud resistivities. For optimum performance, the invaded zone resistivity should be about twice the formation resistivity. The SFL tool measures the zone influenced by fluids that have invaded the formation from the borehole (called the invaded zone). Thus, if drilling-fluid resistivity is known, then estimates of porosity and qualitative permeability can be derived from a combination of the SFL and ILD measurements. Generally, the ILD has the greatest depth of investigation and thus is considered to give the best estimate of true formation resistivity in formations having a resistivity less than about 50 ohm. Depths of investigation of

the ILD, ILM, and SFL are 5, 2.5, and 0.5 m, respectively, and vertical resolution is 1.5 m.

Induction measurements are, strictly speaking, measurements of formation conductivity that are converted to resistivity values for ease of presentation. Induction is measured using a system of transmitter/receiver coil pairs. An alternating current (10, 20, or 40 kHz) is produced in the transmitter coils, inducing eddy currents in the formation. The magnetic field produced by these circulating eddy currents in turn induces a voltage at the receiver coil. The magnitude of the eddy current flow, and hence the receiver voltage and current, is proportional to the formation conductivity.

The DITE tool records both a formation response signal R (90° out of phase) and a noise signal X (180° out of phase) and thus allows us to process and obtain a more accurate reading of formation conductivity. The SFL uses a focusing configuration and constant potential electrodes and thus obtains a shallow, focused resistivity measurement.

The DIT-D is the analog version of the DITE. Only alternating current at 20 kHz is used in the transmitter coils.

Natural Gamma-Ray Spectroscopy Tool (Natural Gamma-Ray)

A basic gamma ray (GR) records the natural radioactivity of a formation using a scintillation detector. This radiation is recorded initially as counts per second and is subsequently presented in terms of American Petroleum Institute (API) radiation units. The natural gamma-ray tool (NGT) allows for the total gamma-ray response (SGR) of a formation to be separated into three components: the contributions from K, U, and Th. The analysis is achieved by subdividing the entire incident gamma-ray spectrum into five discrete energy windows. The total counts recorded in each window, for a specified depth in the well, are processed at the surface to give the relative elemental abundance of K, U, and Th. The depth of investigation depends on formation density and energy of the gamma rays emitted. For higher-energy gamma rays in low-density formations, most of the signal will come from the first 50 cm away from the borehole wall, while lower-energy gamma rays in high-density formations will have a smaller radius of investigation. The use of KCl in the drilling fluid (used for shale control) will affect log readings, and should be corrected for.

Mechanical Caliper Device

The mechanical caliper device (MCD) is a tool that provides a basic two-dimensional caliper log of the borehole by means of a bowspring-mounted measurement system. The hole diameter (HD) log is used to detect washouts or constrictions. Borehole diameter significantly affects many of the other logging measurements, and hole diameter is an important factor in log correction routines. The maximum measurable hole size is 30 in. (0.76 m).

Compensated Neutron Tool (Model G)

Neutrons (4 to 6 MeV) from an americium-beryllium (Am-Be) source collide with hydrogen (H) in the formation and lose energy. These slowed neutrons are then captured by chlorine (Cl), lithium (Li), boron (B), and gadolinium (Gd), and captured gamma rays are emitted. Thus, the H content (both bound and free) of the formation is the primary quantity obtained with this tool, and this is expressed as thermal neutron porosity. The epithermal (intermediate energy) neutron flux is an indicator of free water only, which is expressed as epithermal neutron porosity. The difference between thermal neutron porosity and epithermal neutron porosity is thus proportional to bound water in clays in the formation. The vertical resolution of this tool is approximately 0.3 m, and beds of less than 1 m thick will give less

than true readings. The radius of investigation decreases with increasing porosity from about 0.6 m at zero porosity to about 0.2 m at 30% porosity for a 6-in. (0.15-m)-diameter hole. The readings are affected by neutron absorbers, such as Cl, in the borehole and pore spaces, which should be corrected for accordingly.

Litho-Density Tool

The ^{137}Cs source in the LDT emits gamma rays with an energy of 66 keV that interact with the electrons in the formation by Compton scattering. This transfer of energy forms the basis of the density measurement. Formation density is calculated from this energy flux by assuming that the atomic weight of most rock-forming elements is approximately twice their atomic number. At low energies, gamma radiation is absorbed by the photoelectric effect. The photoelectric factor (PEF) is used primarily as a matrix mineralogy indicator. The depth of investigation is approximately 0.12 m, with a vertical resolution of about 0.25 m. Thus, this tool measures the invaded zone in porous and permeable formations. The presence of barite in the drilling fluid will affect the PEF reading and ideally should be corrected for in cases of thick mudcake and/or hole rugosity.

Gamma-Ray Spectroscopy Tool

Thermal neutrons (14 MeV) generated by the GST interact with the formation and are captured by Ca, Cl, Si, Fe, H, and S, with the resulting emission of captured gamma rays. This gamma radiation is measured by an NaI detector, and the spectrum is windowed for the energies of the individual elements. Since other elements contribute somewhat to the signal, only various elemental ratios are used at sea as preliminary indicators of lithology, porosity, clay-mineral content, pore-fluid salinity, and evaporite content. In post-cruise processing, a linear inversion method is used to obtain the dry weight percent as oxides for each of the six elements above.

Aluminum Clay Tool

The ACT is a modified NGT tool paired with a modified CNT-G carrying a californium (Cf) source (2 MeV). The radiation emitted by this source primarily activates the Al, Mn, and Ca in the formation. The modified NGT measures the induced plus background activity to determine the Al and Mn concentrations. The ACT data, combined with the GST logs, are routinely used to determine clay mineralogy and to detect the presence of hydrothermal alteration and vein-filling minerals (E. Pratson, pers. comm., 1988).

Standard Gamma-Ray Tool

The SGT measures gamma-ray radiation in a total-spectrum window. Thus, no distinction can be made among K, U, and Th with this tool.

Telecommunications Cartridge

The telecommunications cartridge (TCC) is located at the top of each tool string and channels the data from all the tools to the surface.

Synthetic Seismograms

Synthetic seismograms are generated from logging data obtained with the LSS or SDT tools. As many as eight individual logs are used in the process: four transit time measurements from near and far receivers, two slowness logs calculated from these transit times, an electrical resistivity log, and a bulk density log. If no density log is available, a pseudo-density log can be created using the data obtained from core measurements.

These logs are initially examined for continuity and quality. An interval is chosen where the four transit time logs are all sim-

ilar and contain no noise spikes. In this case, the two slowness curves (for near and far receiver combinations) are considered accurate, and the transit time logs can be ignored. If discontinuities or noise spikes occur in the transit time logs, they can be edited (if few in number) or reprocessed using software that truncates noise spikes and/or discards data from one or more receivers for a given interval. In either case, the resulting slowness logs must be examined carefully to be considered accurate. In general, the two slowness logs are nearly identical, and one will not be used in the synthetic seismogram generation.

The interval from seafloor to the first quality log data is replaced with a smooth ramp having slowness values that begin at 190 $\mu\text{s}/\text{ft}$ (slowness of water) at the seafloor and gradually decrease to the value of the first log data point. In this way, the synthetic seismogram will begin at seafloor and will contain no spurious reflectors in the unlogged interval.

The bulk density log from the LDT or a pseudo-log created from laboratory measurements is required in addition to the slowness log. In many cases, a simple constant density log can be generated using the average value of the laboratory data, providing the range is small. Experience shows that this often gives surprisingly good results. If laboratory data from discrete measurements are used, some form of averaging or smoothing is necessary to create a continuous density log.

The slowness and density logs are used in the program to generate an impedance log (velocity \times density), which is convolved with a zero-phase Ricker wavelet. The frequency of this wavelet can be varied, depending on the source generating the original seismic profile. A 30-Hz wavelet is capable of a vertical resolution on the order of 30 m; thus, reflectors cannot generally be attributed to any small-scale lithologic horizons.

A synthetic seismogram is plotted with two-way traveltime on the left scale and depth below seafloor on the right. Impedance contrasts create positive or negative peaks, indicating reflectors. An artifact of the convolution process is an extra interval of data on the synthetic seismogram, which is on the order of one wavelength of the selected Ricker wavelet. This data should be disregarded. However, the depth scale on the right indicates the depths of logging data and is correct.

VERTICAL SEISMIC PROFILING

Vertical seismic profiling (VSP) is a downhole geophysical experiment that involves clamping a geophone or seismometer in the borehole at different depths and recording the seismic wavefield generated from a source at the surface vertically above the geophone. This allows for the direct measurement of the *in-situ* behavior of the wavefields as they propagate through the earth surrounding the borehole. A seismometer records both the direct, downgoing waves as well as upgoing waves reflected from acoustic impedance changes below the clamping depths. Processing techniques can be applied to separate the upgoing from the downgoing wavefields. Detailed interval velocities between received depths can be calculated from differences in the arrival time of the direct wave. Analyses of the measured wavefields are used for correlation with subsurface stratigraphic relationships, lithological conditions, and rock properties determined from the cores and other geophysical logs. The seismograms produced closely approximate conventional seismic profiles. Thus, these seismograms provide a means for making a direct correlation between borehole information and seismic-reflection profiles at the site, i.e., to determine the depth to various seismic reflections and to determine what physical properties produce the reflections. This information allows for an extrapolation of borehole results regionally. The data also can be used to predict the acoustic properties and the depth to interfaces below the total depth of the hole.

The seismometer used for this experiment is a three-component tool provided by Woods Hole Oceanographic Institution (WHOI). The receiver is a Geospace all-lock seismometer, which has three sets of two geophones in series orthogonally configured with two components in the horizontal plane and one in the vertical plane. The tool is clamped to the borehole using an arm that is activated from the ship. Two separate sound sources are used: (1) a small 400-in.³ water gun (SSI S400 Model), and (2) a larger 1000-in.³ air gun (Bolt Model PAR 1500), both operated with approximately 1900-psi air pressure. These guns are suspended 4.6 and 6.7 mbsl, respectively. The small air gun provides higher-frequency energy for better resolution of the shallower sedimentary section, while the large air gun provides lower-frequency energy for penetration into the deeper sedimentary section and basement. A source monitor hydrophone is suspended at 250 mbsl to collect the source signature for each shot, which is used to process these data at a later time. The three seismic signals plus the source monitor are recorded digitally using the HIGHRES logging program installed on a Masscomp M-500 minicomputer located in the underway geophysics laboratory. The Masscomp system is triggered by a blast phone hung between the guns. The digital data are written as 32-bit IBM floating point data in SEG Y format on a nine-track tape. An eight-channel Hewlett-Packard audio tape recorder is used as a backup analog recording system.

The tool is lowered to the bottom of the hole using the logging winch and cable and clamped in place. The guns are shot successively until enough good shots have been recorded (5 to 10) for each source. Signal quality is monitored from the underway geophysics laboratory. The tool is then unclamped, and the procedure repeated at 12- to 24-m intervals uphole. Good data usually can be obtained even through a cased hole if bonding between the formation and casing is adequate.

Seismic data collected from a VSP experiment are preliminarily processed on board the ship using the shipboard VAX 11/750 computer. The SEG Y tapes generated on the Masscomp acquisition system are reformatted to ROSE format to use processing programs developed by WHOI. Shots are sorted by gun type and receiver depth and then stacked. Seismograms are plotted for comparison with borehole information, seismic-reflection data, and for calculation of interval velocities.

HEAT FLOW MEASUREMENTS

Introduction

Factors that control heat flow in the oceanic crust are complicated by variations in the thermal budget associated with different morphotectonic provinces. The net thermal budget may be a function of a variety of heat sources and sinks, age, and location with respect to major plate boundaries, tectonic movements, or mass wasting, and finally, pore-fluid circulation within the oceanic crust and sediments. Measuring temperatures in oceanic boreholes enhances our understanding of how heat-transfer mechanisms operate.

Methodology

The temperature logging tool (TLT), designed by the Borehole Research Group at the Lamont-Doherty Geologic Observatory, is a low-temperature tool that records temperature and pressure data while attached to the bottom of another logging tool, either a Schlumberger tool, the BHTV tool, or the multi-channel sonic (MCS) tool. This avoids the necessity of conducting a separate logging run to measure low temperatures. Instead of transmitting data up the logging wireline cable, temperature and pressure data are recorded internally within the tool. Actual logging is pressure activated at a pre-selected depth, usually

200 m above the seafloor. Once the TLT starts logging, three measurements (two temperature and one pressure) are recorded every 0.5 s. One of the temperature readings is from a fast response thermistor, and the other is from a stable, highly accurate thermistor. At the surface, the TLT data are later merged with Schlumberger depth data to generate a temperature vs. depth curve.

Thermal Equilibrium Corrections

The thermal gradient upon which heat flow values are determined is based on temperature logs collected after the borehole has reached equilibrium. In most cases, this is logistically impractical. To circumvent this problem, Jaeger (1961) and later Burch and Langseth (1981) developed a method of estimating the thermal equilibrium gradient by taking into account the magnitude of thermal disturbances produced by drilling and hole circulation. This correction can be further constrained by conducting several temperature logging runs over a series of days, which is possible if a large logging program is scheduled.

Heat Flow Calculations

Actual heat flow is determined using the following equation,

$$Q = \delta T / \delta z \cdot C,$$

where Q is heat flow with units of mW/m^2 , $\delta T / \delta z$ is the thermal equilibrium gradient in units of K/m (kelvins per meter), and C is thermal conductivity in units of $W/m \cdot K$ (watt per meter kelvin).

Thermal Conductivity Measurements

Thermal conductivity measurements are determined in a variety of ways. On board the *JOIDES Resolution*, thermal conductivity is measured directly from the cores in the physical properties laboratory (see "Physical Properties" section, this chapter). A more robust method for calculating thermal conductivity uses measured porosity and volume fraction of mineral components, based on a continuous mineralogical profile derived from specialized geochemical and geophysical wireline logs (Wollenberg and Smith, 1987). This technique provides the means of correlating thermal gradients with possible variations in thermal conductivity, while *in-situ* measurements of K , Th , and U concentrations can be used to constrain the timing and magnitude of hydrothermal activity within the oceanic crust. Geochemical and geophysical logs at Sites 765 and 766 were collected using Schlumberger downhole logging tools (see "Geophysical Well Logging" section, this chapter).

PERMEABILITY MEASUREMENTS

Introduction

In-situ permeability measurements have been successfully completed in DSDP Holes 395A and 504B and ODP Hole 735B (Anderson and Zoback, 1982; Becker et al., 1983; Hickman et al., 1984; Anderson et al., 1985; Becker et al., 1988). These experiments provided the means of addressing the nature of circulation of seawater and other pore fluids through the oceanic crust. The modes and effects of circulation may be largely controlled by the variable permeability and porosity of the basaltic and gabbroic formations that constitute the oceanic crust. This variation in permeability may be related to irregular fractures and porous spaces of unknown dimensions. Therefore, continued *in-situ* measurements of bulk permeability and porosity at large enough scales to recover these hydrologic properties are essential.

Methodology

The optimal means of determining bulk permeability is by actively testing the formation *in-situ* with steel-reinforced inflatable packers, which hydraulically seal a section of the borehole (Fig. 16). By applying a differential pressure to an isolated section, the following hydrologic properties can be measured: pore pressure, transmissivity (from which permeability can be derived), and the storage coefficient (which is closely related to bulk formation porosity). These properties are determined from pressure measurements during two types of tests:

1. Pulse tests, in which downhole pressure recorders monitor the decay of a short, effectively instantaneous pressure pulse applied to the formation. In a relatively impermeable forma-

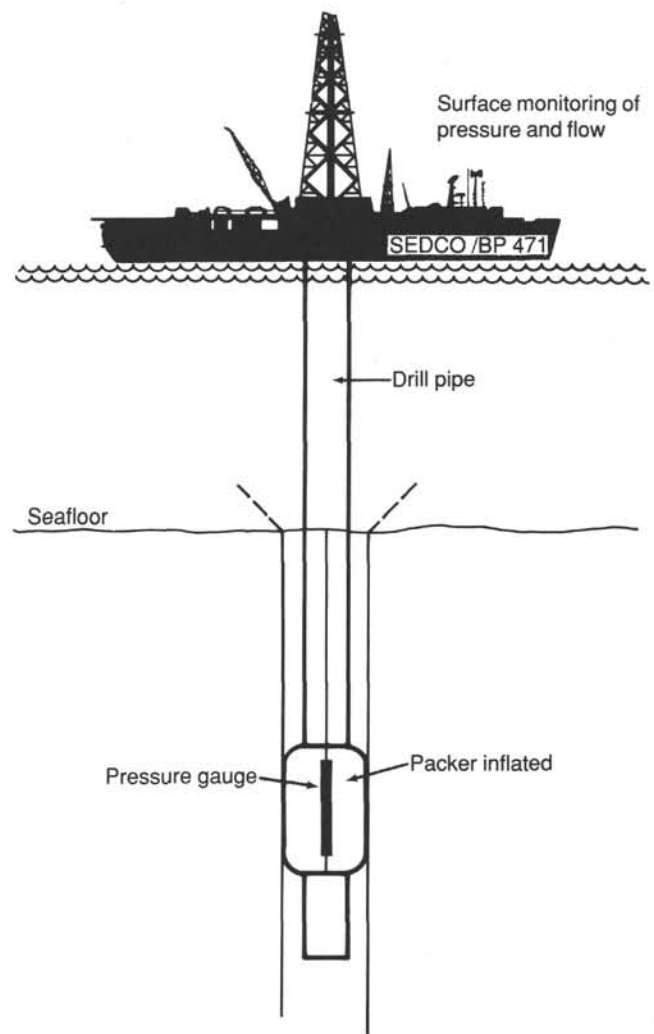


Figure 16. Schematic representation of the permeability operations showing the inflatable packer downhole in the inflated position. The pressure is monitored both downhole and at the surface to ensure data coverage. Flow meters near the mud and cement pumps are used to control the flow rates in the case of the constant flow tests. An attempt to hydrofrac the formation was planned at the end of the permeability tests. The permeability program for Leg 123 used the rotating packer system, which can be assembled and placed in the hole (in the deflated mode) during the Schlumberger, BHTV, and VSP logging. This is possible because these tools can pass through the rotating packer, thus saving an extra pipe trip.

tion, the period of decay is long compared to the duration of the pulse, and permeability can be determined using the theory for an instantaneous pulse (Papadopoulos et al., 1973; Bredehoft and Papadopoulos, 1980). In permeable formations, a pressure pulse will decay rapidly, and a flow test must be run.

2. Constant flow tests, in which downhole pressure recorders monitor a fairly steady pressure while fluids are pumped into the formation at a constant rate. If steady state is reached, permeability can be estimated using Darcy's law (e.g., Matthews and Russell, 1967).

REFERENCES

- Aita, Y., 1987. Middle Jurassic to Lower Cretaceous radiolarian biostratigraphy of Shikoku with reference to selected sections in Lombardy, Basin, and Sicily. *Geology*, 58(1):91-115.
- Anderson, R. N., and Zoback, M. D., 1982. Permeability, underpressures, and convection in the oceanic crust near the Costa Rica Rift, eastern equatorial Pacific. *J. Geophys. Res.*, 87:2860-2868.
- Anderson, R. N., Zoback, M. D., Hickman, S. H., and Newmark, R. L., 1985. Permeability vs. depth in the upper oceanic crust: *in-situ* measurements in DSDP Hole 504B, eastern equatorial Pacific. *J. Geophys. Res.*, 90:3659-3669.
- Apthorpe, M., 1988. Cainozoic depositional history of the North West Shelf. In Purcell, P. G., and Purcell, R. R. (Eds.), *The North West Shelf, Australia: Proc. Pet. Explor. Soc., Australia, Symp.*, 55-84.
- Aubry, M. P., Berggren, W. A., Kent, D. V., Flynn, J. J., Klitgord, K. D., Obradovich, J. D., and Prothero, D. R., 1988. Paleogene geochronology: an integrated approach. *Paleoceanography*, 3(6):707-742.
- Bartenstein, H., and Brand, E., 1951. Mikropalaontologische Untersuchungen zur Stratigraphie des nordwestdeutschen Valendis. *Senckenb. Naturf. Ges. Abhandl.*, 485:239-336.
- Baumgartner, P. O., 1984. A Middle Jurassic-Early Cretaceous low-latitude radiolarian zonation based on unitary associations and age of Tethyan radiolarites. *Eclog. Geol. Helv.*, 77(3):729-836.
- , 1987. Age and genesis of Tethyan Jurassic radiolarites. *Eclog. Geol. Helv.*, 80(3):831-879.
- Becker, K., Langseth, M. G., Von Herzen, R. P., and Anderson, R. N., 1983. Deep crustal geothermal measurements, Hole 504B, Costa Rica Rift. *J. Geophys. Res.*, 88:3447-3457.
- Becker, K., Sakai, H., et al., 1988. *Proc. ODP, Init. Repts.*, 111: College Station, TX (Ocean Drilling Program).
- Belford, D. J., 1981. Late Cretaceous planktonic foraminifera in Valdivia core KL1 from the Scott Plateau and Rowley Terrace, off northwestern Australia. *Bur. Min. Res., Australia, Bull.*, 213:48-67.
- Bell, J. S., and Gough, D. I., 1979. Northeast-southwest compressive stress in Alberta: evidence from oil wells. *Earth Planet. Sci. Lett.*, 45:475-482.
- Berggren, W. A., 1969. Cenozoic chronostratigraphy, planktonic foraminiferal zonation, and the radiometric time scale. *Nature*, 224:1072-1075.
- Berggren, W. A., Kent, D. V., and Flynn, J. J., 1985a. Jurassic to Paleogene: Part 2 Paleogene geochronology and chronostratigraphy. In Snelling, N. J., (Ed.), *The Chronology of the Geologic Record*. Geol. Soc. (London) Mem., 10:141-195.
- Berggren, W. A., Kent, D. V., and Van Couvering, J.A., 1985b. The Neogene: Part 2. Neogene geochronology and chronostratigraphy. In Snelling, N. J., (Ed.), *The Chronology of the Geologic Record*. Geol. Soc. (London) Mem., 10:211-260.
- Blanton, L., 1983. The relationship between recovery deformation and *in-situ* stress magnitudes. *Soc. Pet. Eng.*, 11624.
- Blow, W. H., 1969. Late middle Eocene to Holocene planktonic foraminiferal biostratigraphy. In Bronnmann, P., and Renz, H. H. (Eds.), *Proc. 1st Int. Conf. Planktonic Microfossils*, 1:199-422.
- , 1979. *The Cainozoic Globigerinida* (3 Vols.). In Brill, E. J. (Ed.): Leiden.
- Bown, P. R., 1987. Taxonomy, evolution, and biostratigraphy of Late Triassic-Early Jurassic calcareous nannofossils. *Spec. Pap. Palaeontol.*, 38:1-118.
- Bown, P. R., Cooper, M.K.E., and Lord, A. R., 1988. A calcareous nannofossil zonation scheme for the early to mid-Mesozoic. *Newsl. Strat.*, 20:91-114.
- Bown, P. R., and Lord, A. R., in press. The occurrence of calcareous nannofossils in the Triassic-Jurassic boundary interval. *Proc. Triassic/Jurassic Boundary Working Group*, Lyon.
- Boyce, R. E., 1976. Definition and laboratory techniques of compressional sound velocity parameters and wet-water content, wet-bulk density, and porosity parameters by gravimetric and gamma-ray attenuation techniques. In Schlanger, S. O., Jackson, E. D., et al., *Init. Repts. DSDP*, 33: Washington (U.S. Govt. Printing Office), 931-958.
- , 1977. Deep Sea Drilling Project procedures for shear strength measurements of clay sediment using modified Wykeham-Farrance laboratory vane apparatus. In Barker, P. E., Dalziel, I.W.D., et al., *Init. Repts. DSDP*, 36: Washington (U.S. Govt. Printing Office), 1059-1068.
- Bralower, T. J., 1987. Valanginian to Aptian calcareous nannofossil stratigraphy and correlation with the upper M-sequence magnetic anomalies. *Mar. Micropaleontol.*, 11:293-310.
- Bredehoft, J. D., and Papadopoulos, S. S., 1980. A method for determining the hydraulic properties of tight formation. *Water Resour. Res.*, 16:223-238.
- Brewer, P. G., and Spencer, D. W., 1971. Colorimetric determination of manganese in anoxic waters. *Limnol. Oceanogr.*, 16:107.
- Bukry, D., 1981. Pacific Coast coccolith stratigraphy between Point Conception and Cabo Corientes, Deep Sea Drilling Project, Leg 63. In Yeats, R. S., Haq, B. U., et al., *Init. Repts. DSDP*, 63: Washington (U.S. Govt. Printing Office), 445-471.
- Burch, T. K., and Langseth, M. G., 1981. Heat-flow Determination in three DSDP boreholes near the Japan Trench. *J. Geophys. Res.*, 86:9411-9419.
- Caron, M., 1985. Cretaceous planktonic foraminifers. In Bolli, H. M., Saunders, J. B., and Perch-Nielsen, K. (Eds.), *Plankton Stratigraphy*: Cambridge (Cambridge Univ. Press), 17-86.
- Carter, D.J.T., 1980. *Echo-Sounding Correction Tables*: Taunton (Hydrogr. Dept., Ministry of Defense).
- Casey, R. E., and Reynolds, R. A., 1980. Late Neogene radiolarian biostratigraphy and paleoceanography with suggested cosmopolitan radiolarian datums. *Cush. Found. Spec. Pub.*, 19:287-300.
- Chaproniere, G.C.H., 1981. Late Oligocene to early Miocene planktonic foraminifers from Ashmore Reef No. 1 well, northwest Australia. *Alcheringa*, 5:103-131.
- Chen, P.-Y., 1977. *Table of Key Lines in X-Ray Powder Diffraction Patterns of Minerals in Clays and Asspcoated Rocks*. U.S. Geol. Surv. Pap. 21.
- Cooper, M.K.E., 1984. Nannofossils across the Jurassic/Cretaceous boundary in the Tethyan realm. *Int. Symp. Jurassic Stratigr.*, 2:429-443.
- Dailey, D. H., 1983. Late Cretaceous and Paleocene benthic foraminifers from Deep Sea Drilling Project Site 516, Rio Grande Rise, western South Atlantic Ocean. In Barker, P. F., Carlson, R. L., Johnson, D. A., et al., *Init. Repts. DSDP*, 72: Washington (U.S. Govt. Printing Office), 757-782.
- Emeis K., and Kvenvolden, K. A., 1986. *Shipboard Organic Geochemistry on JOIDES Resolution*: College Station, TX (Ocean Drilling Program), ODP Tech. Note, 7.
- Espitalié, J., Madec, M., and Tissot, B., 1977. Source rock characterization method for petroleum exploration. *Proc. Offshore Tech. Conf.*, 3:439-443.
- Fisher, R. V., and Schmincke, H.-U., 1984. *Pyroclastic Rocks*: Berlin (Springer Verlag).
- Gartner, S., Jr., 1977. Calcareous nannofossil biostratigraphy and revised zonation of the Pleistocene. *Mar. Micropaleontol.*, 2:1-25.
- Geroch, S., and Nowak, W., 1984. Proposal of zonation for the late Tithonian to late Eocene, based upon arenaceous foraminifera from the outer Carpathians, Poland. In Oertli, H. J. (Ed.), *Benthos '83: 2nd Int. Symp. on Benthonic Foraminifers*, 225-239.
- Gieskes, J. M., 1974. Interstitial water studies, Leg 25. In Simpson, E. S., Schlich, R., et al., *Init. Repts. DSDP*, 81: Washington (U.S. Govt. Printing Office), 669-673.
- Gieskes, J. M., and Peretsman, G., 1986. *Procedures of Interstitial Water Analyses on the SEDCO BP/471—Some Comments*: College Station, TX (Ocean Drilling Program), ODP Tech. Note No. 5.
- Gradstein, F. M., 1978. Biostratigraphy of Lower Cretaceous Blake Nose and Blake-Bahama foraminifers, DSDP Leg 44, western North At-

- lantic. In Benson, W. E., Sheridan, R. E., et al., *Init. Repts. DSDP*, 44: Washington (U.S. Govt. Printing Office), 663-701.
- _____, 1983. Paleogeology and stratigraphy of Jurassic abyssal foraminifera in the Blake Bahama Basin, Deep Sea Drilling Project Site 534. In Sheridan, R. E., Gradstein, F. M., et al., *Init. Repts. DSDP*, 76: Washington (U.S. Govt. Printing Office), 537-559.
- _____, 1986. Northwestern Atlantic Mesozoic Biostratigraphy. In Vogt, P. R., and Tucholke, B. E. (Eds.), *The Geology of North America, Vol. M, The Western North Atlantic Region*: Tulsa (Geol. Soc. Am.), 507-525.
- Gradstein, F. M., Agterberg, F. P., Aubry, M. P., Berggren, W. A., Flynn, J. J., Hewitt, R., Kent, D. V., Klitgord, K. D., Miller, K. G., Obradovich, J., Ogg, J. G., Prothero, D. R., and Westermann, G.E.G., 1988. Chronology of fluctuating sea levels since the Triassic. *Science*, 241:599-601.
- Haimson, B. C., and Fairhurst, C., 1970. In-Situ Stress determination at great depth by means of hydraulic fracturing. *Proc. 11th Symp. Rock Mech.*, 559-589.
- Hansen, J. M., 1977. Dinoflagellate stratigraphy and echinoid distribution in Upper Maastrichtian and Danian deposits from Denmark. *Bull. Geol. Soc. Denmark*, 26:1-26.
- Hart, M., 1984. The superfamily Robertinacea in the Lower Cretaceous of the U.K. and adjacent areas of northwest Europe. In Oertli, H. J. (Ed.), *Benthos '83: 2nd Int. Symp. Benthic Foraminifers*, 289-298.
- Helby, R., Morgan, R., and Partridge, A. D., 1987. A palynological zonation of the Australian Mesozoic. *Mem. Assoc. Australasian Paleontologists*, 4:1-94.
- Herb, R., and Scheibnerova, V., 1977. Synopsis of Cretaceous planktonic foraminifers from the Indian Ocean. In Heirtzler, J. R., Bolli, H. M., Davies, T. A., Saunders, J. B., and Sclater, J. G. (Eds.), *Indian Ocean Geology and Biostratigraphy*: Washington (Am. Geophys. Un.), 399-415.
- Hickman, S. H., Langseth, M. G., and Svitek, J. F., 1984. In-situ permeability and pore-pressure measurements near the Mid-Atlantic Ridge, Deep Sea Drilling Project Hole 395A. In Hynman, R. D., Salisbury, M. H., et al., *Init. Repts. DSDP*, 78B: Washington (U.S. Govt. Printing Office), 699-708.
- Hubbert, M. K., and Willis, D. G., 1957. Mechanics of hydraulic fracturing. *Trans. AIME*, 210:153-160.
- Jaeger, J. C., 1961. The effect of drilling fluid on temperatures measured in boreholes. *J. Geophys. Res.*, 66:563-569.
- Kennett, J. P., and Srinivasan, M. S., 1983. *Neogene Planktonic Foraminifera, a Phylogenetic Atlas*: Stroudsburg (Hutchinson Ross).
- Kent, D. V., and Gradstein, F. M., 1985. A Cretaceous and Jurassic geochronology. *Geol. Soc. Am. Bull.*, 96(11):1419-1427.
- Kowallis, B. J., and Wong, H. F., 1983. Microcrack study of granitic cores from Illinois deep borehole UPH3. *J. Geophys. Res.*, 88:7373-7380.
- Krashennikov, V. A., 1974. Upper Cretaceous benthonic agglutinated foraminifers, Leg 27, Deep Sea Drilling Project. In Veevers, J. J., Heirtzler, J. R., et al., *Init. Repts. DSDP*, 27: Washington (U.S. Govt. Printing Office), 631-661.
- Kuznetsova, K. L., 1974. Distribution of benthonic foraminifera in Upper Jurassic and Lower Cretaceous deposits at Site 261, DSDP Leg 27, on the eastern Indian Ocean. In Veevers, J. J., Heirtzler, J.R., et al., *Init. Repts. DSDP*, 27: Washington (U.S. Govt. Printing Office), 523-534.
- Kvenvolden, K. A., and McDonald, T. J., 1986. *Organic Chemistry on the JOIDES Resolution—An Assay*: College Station, TX (Ocean Drilling Program), Tech. Note No. 6.
- Lee, H. J., 1984. State of the art: laboratory determination of strength of marine soils. In Chaney, R. C., and Demars, K. R. (Eds.), *Strength Testing of Marine Sediments: Laboratory and In-Situ Measurements*. ASTM Spec. Tech. Publ. 883, 181-250.
- Manheim, F. T., and Sayles, F. L., 1974. Composition and origin of interstitial waters in marine sediments, based on deep sea drill cores. In Goldberg, E. D. (Ed.), *The Sea, Marine Chemistry*: New York (Wiley), 5:527-568.
- Martini, E., 1971. Standard Tertiary and Quaternary calcareous nannoplankton zonation. In Farinacci, A. (Ed.), *Proc. 2nd Planktonic Conf.*, 2:739-785.
- Matthews, C. S., and Russell, D. G., 1967. *Pressure Build-Up and Flow Tests in Wells*: Dallas, TX (Soc. Pet. Eng. AIME), Mono. 1.
- Mazzullo, J. M., Meyer, A., and Kidd, R., 1988. New Sediment Classification Scheme for the Ocean Drilling Program. In Mazzullo, J. M., and Graham, A. G. (Eds.), *Shipboard Sedimentologists' Handbook*, ODP Tech. Note 8.
- McGowan, B., 1977. Maastrichtian to Eocene foraminiferal assemblages in the northern and eastern Indian Ocean region: correlations and historical patterns. In Heirtzler, J. R., Bolli, H. M., Davies, T. A., Saunders, J. B., and Sclater, J. G. (Eds.), *Indian Ocean Geology and Biostratigraphy*: Washington (Am. Geophys. Un.), 417-458.
- McMinn, A., 1988a. The Cretaceous-Tertiary boundary in the Bonaparte Basin, northwestern Australia. *Proc. 7th Int. Palynol. Congr., Brisbane*. (Abstract)
- _____, 1988b. Outline of a Late Cretaceous dinoflagellate zonation of northwestern Australia. *Alcheringa* 12:137-156.
- Moullade, M., 1984. Intérêt des petits foraminifères benthiques "profonds" pour la biostratigraphie et l'analyse des paléoenvironnements océaniques mésozoïques. In Oertli, H. J. (Ed.), *Benthos '83: 2nd Int. Symp. Benthic Foraminifers*, 429-464.
- Moullade, M., Kuhnt, W., and Thurow, J., 1988. Agglutinated benthic foraminifers from Upper Cretaceous variegated clays of the North Atlantic Ocean. In Boillot, G., Winterer, E. L., et al., *Proc. ODP, Sci. Results*, 103: College Station, TX (Ocean Drilling Program), 349-377.
- Munsell Soil Color Charts, 1975. Baltimore (Munsell Color).
- Norrish, K., and Hutton, J. T., 1969. An accurate X-ray spectrographic method for the analysis of a wide range of geological samples. *Geochim. Cosmochim. Acta*, 33:431-453.
- Nur, A., and Simmons, G. 1970. The origin of small cracks in igneous rocks. *Int. J. Rock Mech. Min. Sci.*, 7:307-314.
- Ogg, J. G., 1984. Comment on "Magnetostratigraphy of the Jurassic-Cretaceous boundary in the Maiolica limestone (Umbria, Italy)." *Geology*, 12:701-702.
- Ogg, J. G., and Lowrie, W., 1986. Magnetostratigraphy of the Jurassic/Cretaceous boundary. *Geology*, 14:547-550.
- Ogg, J. G., and Steiner, M. B., in press. Late Jurassic and Early Cretaceous magnetic polarity time scale. *Proc. Jurassic Stratigr. Symp.*
- Okada, H., and Bukry, D., 1980. Supplementary modification and introduction of code numbers to the low-latitude coccolith biostratigraphic zonation (Bukry, 1973; 1975). *Mar. Micropaleontol.*, 5(3): 321-325.
- Papadopoulos, S. S., Bredehoeft, J. D., and Cooper, H. H., 1973. On the analysis of slug test data. *Water Resour. Res.*, 9:1087-1089.
- Pessagno, E. A., 1977. Lower Cretaceous radiolarian biostratigraphy of the Great Valley sequence and Franciscan complex, California coast ranges. *Cushman Found. Foram. Res. Spec. Publ.*, 15:1-87.
- Presley, B. J., 1971. Techniques for analyzing interstitial water samples. Part 1: determination of minor and major inorganic constituents. In Winterer, E. L., Reidel, W. R., et al., *Init. Repts. DSDP*, 7(Pt. 2): Washington (U.S. Govt. Printing Office), 1749-1755.
- Proto Decima, F. R., 1974. Leg 27 calcareous nannoplankton. In Veevers, J. J., Heirtzler, J. R., et al., *Init. Repts. DSDP*, 27: Washington (U.S. Govt. Printing Office), 589-621.
- Remane, J., Bakalova-Ivanova, D., Borza, K., Knauer, J., Nagy, I., Pop, G., and Tardi-Filáz, E., 1986. Agreement on the subdivision of the standard calpionellid zones defined at the 2nd planktonic conference (Roma, 1970). *Acta Geol. Hung.*, 29(1-2):5-14.
- Reynolds, R. C., 1967. Estimations of mass absorption coefficients by Compton scattering: improvements and extrusions of the method. *Am. Mineral.*, 48:1133-1143.
- Riedel, W., and Sanfilippo, A., 1978. Stratigraphy and evolution of tropical Cenozoic radiolarians. *Micropaleontology*, 23(1):61-96.
- Roth, P. H., 1978. Cretaceous nannoplankton biostratigraphy and oceanography of the northwestern Atlantic Ocean. In Benson, W. E., Sheridan, R. E., et al., *Init. Repts. DSDP*, 44: Washington (U.S. Govt. Printing Office), 731-759.
- Roth, P. H., Medd, A. W., and Watkins, D. K., 1983. Jurassic calcareous nannofossil zonation, an overview with new evidence from Deep Sea Drilling Project Site 534. In Sheridan, R. E., Gradstein, F. M., et al., *Init. Repts. DSDP*, 76: Washington (U.S. Govt. Printing Office), 573-579.
- Ruddiman, W., Sarnthein, M., et al., 1988. *Proc. ODP, Init. Repts.*, 108: College Station, TX (Ocean Drilling Program).
- Sanfilippo, A., and Riedel, W. R., 1985. Cretaceous radiolarians. In Bolli, H. M., Saunders, J. B., and Perch-Nielsen, K. (Eds.), *Plankton Stratigraphy*: Cambridge (Cambridge Univ. Press), 573-630.
- Sanfilippo, A., Westberg-Smith, M. J., and Riedel, W. R., 1985. Cenozoic Radiolaria. In Bolli, H. M., Saunders, J. B., and Perch-Niel-

- sen, K. (Eds.), *Plankton Stratigraphy*: Cambridge (Cambridge Univ. Press), 631-712.
- Schaaf, A., 1981. Late Early Cretaceous radiolarians from Deep Sea Drilling Project Leg 62. In Thiede, J., Vallier, T. L., et al., *Init. Repts. DSDP*, 62: Washington (U.S. Govt. Printing Office), 419-470.
- , 1985. Un nouveau canevas biochronologique du Crétacé Inférieur et moyen: les biozones radiolaires. *Sci. Géol., Bull. Strasbourg*, 38(3):227-269.
- Shamir, G., Zoback, M. D., and Barton, C. A., 1988?. *In-situ* stress orientation near the San Andreas Fault: preliminary results to 2.1 km depth from the Cajon Pass scientific drill hole. *Geophys. Res. Lett.*, 15:131-145.
- Shepard, F., 1954. Nomenclature based on sand-silt-clay ratios. *J. Sed. Petrol.*, 24:151-158.
- Shipboard Scientific Party, 1989. Explanatory Notes. In Haq, B. U., von Rad, U., et al., *Proc. ODP Init. Repts.*, 122: College Station, TX (Ocean Drilling Program), 000-000.
- Sissingh, W., 1977. Biostratigraphy of Cretaceous calcareous nannoplankton. *Geol. Mijnbouw*, 56(1):37-65.
- Sliter, W. V., 1977. Cretaceous benthic foraminifers from the western South Atlantic, Leg 39, Deep Sea Drilling Project. In Supko, P. R., Perch-Nielsen, K., et al., *Init. Rept. DSDP*, 39: Washington (U.S. Govt. Printing Office), 657-698.
- Sliter, W. V., 1980. Mesozoic foraminifers and deep-sea benthic environments from Deep Sea Drilling Project Sites 415 and 416, eastern north Atlantic. In Lancelot, Y., Winterer, E. L., et al., *Init. Repts. DSDP*, 50: Washington (U.S. Govt. Printing Office), 353-428.
- Solorzano, L., 1969. Determination of ammonia in natural waters by phenol hypochlorite method. *Limnol. Oceanogr.*, 14: 799-801.
- Stam, B., 1986. Quantitative analysis of Middle and Late Jurassic foraminifers from Portugal and its implications for the Grand Bank of Newfoundland. *Utrecht Micropaleontol. Bull.*, 34:5-168.
- Staudigel, H. 1980. Chemical analysis of interlaboratory standards. In Donnelly, T., Francheteau, J., Bryan, W., Flower M., Salisbury, M. et al., *Init. Repts. DSDP*, 51-53: Washington, (U.S. Govt. Printing Office), 1331-1333.
- Strickland, J.D.H., and Parsons, T. R., 1968. A manual of seawater analysis. *Bull. Fish. Res. Bd. Canada*, 167:311.
- Teufel, L. W., 1986. *In-situ* stress measurements in inclined holes in the North Sea: applications to water flooding and enhanced oil recovery. *Soc. Pet. Eng. Pap.*, 13986.
- Teufel, L. W., and Warpinski, N. R., 1984. Determination of *in-situ* stress from anelastic strain recovery measurements of oriented cores. *Sandia Rept.*, SAND 84-0512C.
- Tjalsma, R. C., and Lohmann, G. P., 1983. Paleocene-Eocene bathyal and abyssal foraminifers from the Atlantic Ocean. *Micropaleontol. Spec. Publ.* 4.
- Thierstein, H. R., 1971. Tentative Lower Cretaceous nannoplankton zonation. *Eclog. Geol. Helv.*, 64:459-488.
- , 1976. Mesozoic calcareous nannoplankton biostratigraphy of marine sediments. *Mar. Micropaleontol.*, 1:325-362.
- Vacquier, V., 1985. The measurement of thermal conductivity of solids with a transient linear heat source on the plane surface of a poorly conducting body. *Earth Planet. Sci. Lett.*, 74:275-279.
- Van Morkhoven, F.P.C.M., Berggren, W. A., and Edwards, A. S., 1986. Cenozoic cosmopolitan deep-water benthic foraminifers. *Bull. Centres Rech. Explor.-Prod. Elf Aquitaine*, Mem. 11.
- Vincent, E., 1977. Indian Ocean Neogene planktonic foraminiferal biostratigraphy and its paleoceanographic implications. In Heitzler, J. R., Bolli, H. M., Davies, T. A., Saunders, J. B., and Sclater, J. G. (Eds.), *Indian Ocean Geology and Biostratigraphy*: Washington (Am. Geophys. Union), 469-584.
- Voigt, B., 1968. Determination of the virgin state of stress in the vicinity of a borehole from measurements of partial anelastic strain tensor in drill holes. *Felsmech. Ingenieurgeol.*, 6:201-215.
- Von Herzen, R. P., and Maxwell, A. E., 1959. The measurement of thermal conductivity of deep-sea sediments by a needle probe method. *J. Geophys. Res.*, 65, 1557-1563.
- Warpinski, N. R., and Teufel, L. W. 1986. A viscoelastic constitutive model for determining *in-situ* stress magnitudes from anelastic strain recovery of core. *Soc. Pet. Eng. Pap.*, 15368.
- Wentworth, C. K., 1922. A scale of grade and class terms for clastic sediments. *J. Geol.*, 30:377-392.
- Williams, G. L., 1977. Dinocysts: their paleontology, biostratigraphy, and paleoecology. In Ramsey, A.T.S. (Ed.), *Oceanic Micropaleontology*: London (Academic Press), 1231-1325.
- Williamson, M. A., and Stam, B., 1988. Jurassic/Cretaceous Epistominidae from Canada and Europe. *Micropaleontology*, 34:136-158.
- Wollenberg, H. A., and Smith, A. R., 1987. Radiogenic heat production of crustal rocks: an assessment based on geochemical data. *Geophys. Res. Lett.*, 14:295-298.
- Wright, C. A., and Apthorpe, M., 1976. Planktonic foraminiferids from the Maastrichtian of the Northwest Shelf, western Australia. *J. Foramin. Res.*, 6:228-240.
- Zijderveld, J.D.A., Zachariasse, J. W., Verhallen, P. J., and Hilgen, F. J., 1986. The age of the Miocene-Pliocene boundary. *Newsl. Stratigr.*, 16:169-181.
- Zoback, M. D., and Zoback, M. L., 1980. State of stress in the conterminous United States. *J. Geophys. Res.*, 85:6113-6173.
- Zoback, M. D., Zoback, M. L., Mount, V. S., Suppe, J., Eaton, J. P., Healy, J. H., Oppenheimer, D., Reasenber, P., Jones, L., Raleigh, C. B., Wong, I. G., Scotti, O., and Wentworth, C., 1988. New evidence on the state of stress of the San Andreas Fault. *Science*, 238: 1105-1111.

Ms 123A-103